Wood Design FOCUS

A JOURNAL OF CONTEMPORARY WOOD ENGINEERING

Volume 28, Number 2 SUMMER 2018

Theme:
Wood Lateral Resistance System Developments

Editorial

Recent research and analyses have been conducted or are underway for various types of traditional and innovative wood-based lateral systems. This issue of *Wood Design Focus* will provide an overview of recent advancements in these systems to inform the wood design community of these latest developments.

The first paper deals with the force transfer around openings (FTAO) method of shear wall design for wood frame wood structural panel shear walls. Historically, the FTAO method has been considered a last resort in the design industry, due in large part to the fact that an FTAO analysis is more comprehensive and therefore assumed to be more time-consuming than the other two design options. This article will discuss the benefits of FTAO for wood-framed structures, illustrate the testing performed on wood structural panel sheathed wood-framed shear walls for the enhancement of the FTAO methodology, and provide a design example for a wood-framed shear wall with multiple openings and asymmetric wall piers.

Another paper presents the latest successful attempt to develop a low-damage (i.e. resilient) cross-laminated timber (CLT) rocking wall system for mass timber construction in regions of high seismicity. As part of a National Science Foundation funded research project (NHERI Tall Wood Project), a group of researchers and their industry partners designed and tested a full-scale two-story wood building on the outdoor shake table at UC San Diego. The building behaved as expected and withstood 14 earthquakes without significant damage. The details on the design, construction, and testing of the two-story building is outlined in the second article.

For seismic design of multistory platform construction, research of an innovative CLT rocking wall system with an elliptical boundary profile is being conducted. Curvilinear cuts to the load-bearing edges of a rectangular CLT panel produce smoother and more predictable lateral response to earthquakes, with gravity-driven passive re-centering ability and the potential to greatly reduced crushing damage at wall corners. The third paper presents design and full scale cyclic testing performance of a prototype CLT rocking wall with two different types of connections. Hysteresis plots of the test results and idealized analytical models show good agreement between design assumptions and actual properties of the pendulum rocking wall system.

Estimating horizontal deflections of diaphragms comprised of wood structural panels during wind and earthquakes is important for serviceability considerations, building separations and setbacks, and structural integrity evaluation in buildings with large span diaphragms. In smaller light-frame wood buildings, establishing the flexibility of diaphragms relative to adjacent shear walls or frames is necessary to properly classify whether a flexible, rigid or semi-rigid diaphragm approach is valid. In the final paper, the current wood panel diaphragm deflection equation is evaluated, and a new nail-slip contribution formula is mathematically derived that appropriately considers the nail slip contribution for a variety of situations including different panel orientations, different panel sizes, various nail spacings around the same panel, and variable non-linear nail-slip behavior within the same panel. Findings suggest that the current approach significantly underestimates stiffness.

We hope you find this issue of *Wood Design Focus* informative. As always, comments and questions are welcome.

Dr. Thomas D. Skaggs, P.E.
APA-The Engineered Wood Association,
WDF Editorial Board Member

Dr. Shiling Pei, P.E.
Associate Professor,
Colorado School of Mines

Wood Design FOCUS

Published by the
Forest Products Society

Wood Design Focus
(ISSN 1066-5757)
is published quarterly by:
Forest Products Society
251 S.L. White Blvd.
LaGrange, GA 30241
Phone: (706) 443-1337
www.forestprod.org

A complimentary annual subscription is provided to members in good standing of the Forest Products Society (FPS) and the American Wood Council (AWC). Individuals must join either association to receive the publication. Institutions may subscribe for $199 USD per year. Individual articles and past issues may be downloaded from the FPS Knowledge Base at no charge for FPS members and a nominal fee for nonmembers.

The Only FTAO Calculator You Need in Your Toolkit

Jared S. Hensley, P.E.

Introduction

The ratio of sheathing to windows in large buildings has tipped in favor of the windows, reducing the surface area available for wood structural panel sheathing that would otherwise provide the lateral load resistance needed for the building. As trends toward larger buildings with bigger and more numerous windows continue to grow, designers will need a tool they can count on to help them easily calculate the shear walls necessary to resist the lateral forces. The APA Force Transfer Around Openings (FTAO) Calculator helps designers add structural strength and lateral force resistance to buildings with multiple openings.

The FTAO approach is one of three recommended by the American Wood Council (AWC) in their publication *Special Design Provisions for Wind & Seismic* (SDPWS) for designing wood shear walls to resist lateral forces. The other two options include the Individual Full-Height Wall Segments, a more "traditional" approach, and the Perforated Shear Walls, which is an empirical design method based on the percentage of full-height wall segments adjacent to openings. The FTAO method, also referred to as the Force Transfer Shear Walls method, allows the utilization of the full wall geometry, including sheathed areas above and below openings.

Historically, the FTAO method has been considered a last resort in the design industry, due in large part to the fact that an FTAO analysis is more comprehensive and therefore assumed to be more time-consuming than the other two design options. The application of the FTAO method also varies greatly within the industry, as the code simply states that the design must be based on rational analysis. With no clear directive in the design codes, there have been multiple design rationale techniques developed (e.g., Drag-Strut Analogy, Cantilever Beam, Diekmann), which has caused some dispute between design professionals as to which technique is the most precise. These discrepancies are what led APA to perform full-scale wall tests on FTAO design methodology, intended to prove that the application of FTAO can be more practical and simultaneously provide the most design flexibility.

This article will discuss the benefits of FTAO for wood-framed structures, illustrate the testing performed on wood structural panel sheathed wood-framed shear walls for the enhancement of FTAO methodology, and provide a design example for a wood-framed shear wall with multiple openings and asymmetric wall piers.

Benefits of FTAO Wood Shear Walls

There are many benefits to the FTAO method, such as utilizing the entire shear wall geometry to resist the applied load, potentially reducing the number of hold-downs, and reducing the base plate shear anchorage. But the greatest benefit of FTAO over other shear wall design methods lies within the definition of the wall pier aspect ratio.

In the segmented and perforated methods, the aspect ratio of the contributing wall piers is defined as the full height of the wall system divided by the length of the wall pier. (Figure 1, Parts A & B). When utilizing the FTAO method, the aspect ratio of the wall pier is defined as the height of the opening divided by the length of the adjacent wall pier (Figure 1, Part C).

continued on next page

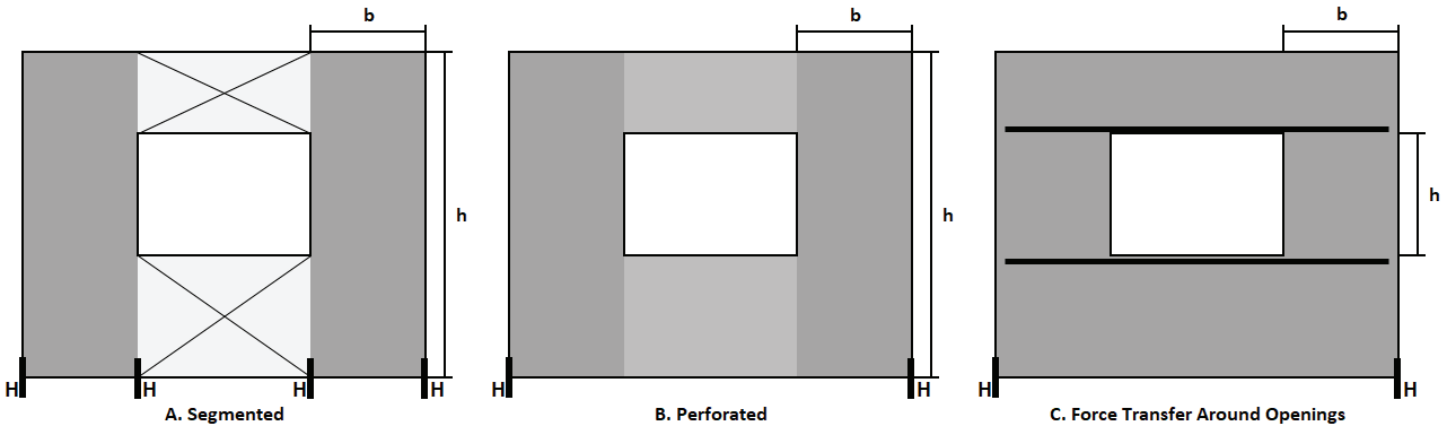

Figure 1: Illustration of aspect ratio (h/b) comparison for all three shear wall methods

For example, given the wall illustrations in Figure 1 where the full height (h) is equal to 10 feet and the opening is 4 feet tall, the minimum wall pier length (b) allowed to be included in the design at the 2:1 aspect ratio for each method would be: segmented and perforated are equal to (10/2) or 5 feet and FTAO is equal to (4/2) or 2 feet. This benefit not only allows for narrower wall segments but also helps increase the overall height of the wall system where other methods might be limited.

This benefit is furthered by utilizing wood structural panel sheathing. The governing aspect ratio limitation in most applicable building codes for wood structural panels is 2:1 with a maximum of 3.5:1 (with the application of an adjustment factor). Although the use of other building materials is permitted, per SDPWS Section 4.3.4 the aspect ratios either cannot exceed 2:1 or a load reduction factor is applied when the aspect ratio surpasses 1:1.

Testing FTAO Design Methodology

FTAO has become more popular amongst design professionals as a viable shear wall analysis for wood-framed walls. The majority of the published FTAO design examples, however, are limited to the wall containing a single opening and, until recently, the recognized FTAO methods were tested in a limited number of installations.

In 2009, a joint research project was conducted by APA–The Engineered Wood Association (APA), the University of British Columbia (UBC) and the USDA Forest Products Laboratory to examine the internal forces generated in wood structural panel sheathed wood-framed shear walls during a lateral event. The test results, in conjunction with analytical computer based models from UBC (twelve full-scale, 8 feet x 12 feet wall configurations) were used to develop an enhanced FTAO design methodology and evaluate the accuracy of the calculated forces in the walls using historic FTAO methods.

The initial testing determined the Diekmann rational analysis as the most accurate simplified method to estimate the forces in the shear wall. Using this approach as the basis, APA expanded the methodology to incorporate multiple openings and asymmetric piers. This methodology is based on the following key design assumptions:

1. The unit shear is equivalent above and below the openings.
2. The corner forces are based on the unit shear above and below the openings and only the wall piers adjacent to that unique opening.
3. The tributary length of the opening is the basis for calculating the shear to each wall pier.
4. The shear to each wall pier is the total shear divided by the length of the wall, multiplied by the sum of the pier length plus the tributary width of the adjacent openings, divided by the pier length: **v1 = (V/L)*((L1 + T1)/L1)**

continued on next page

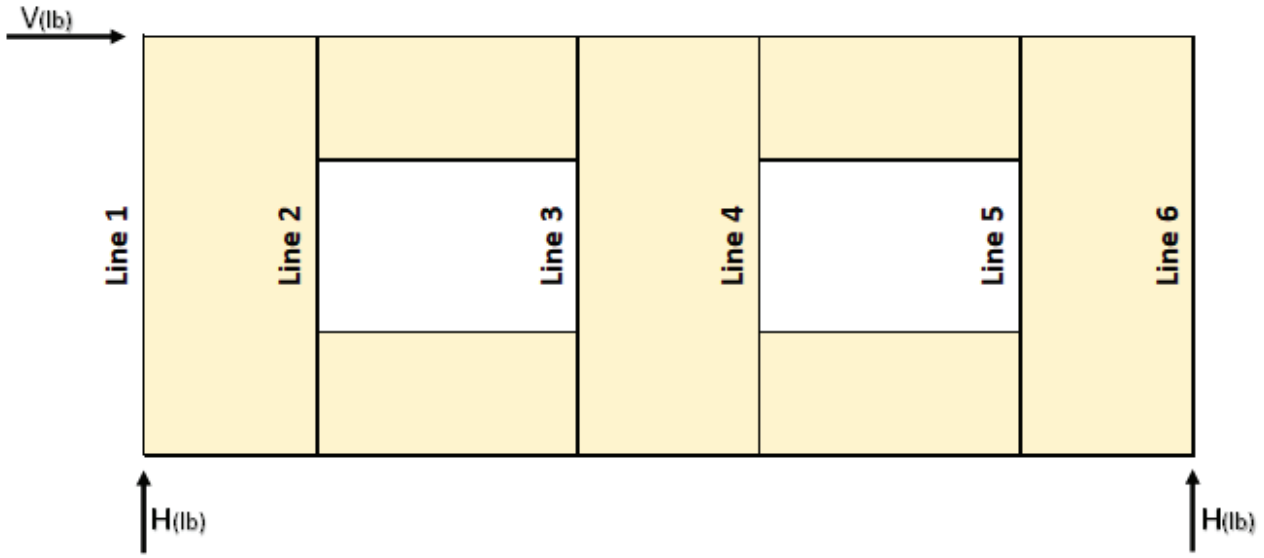

Figure 2: Vertical shear line illustration

5. The unit shear in the corner zones is equal to subtracting the corner forces from the panel resistance, R. R is equal to the shear of the pier multiplied by pier length: **Va1 = (v1L1 - F1)/L1**
6. The design is checked by summing the shears along each vertical line. The first and last lines sum to the hold-down force and the interior lines sum to zero (Figure 2).

Testing data was also used to analyze the overall deflection of the FTAO wall systems, which verified that the sheathing below the openings aided in resisting the overall deflection of the wall. To attain the most accurate fastener deformation variable, the basis of the testing was completed using the four-term deflection equation, 2015 International Building Code (IBC) Equation 23-2:

$$\Delta = \frac{8vh^3}{EAb} + \frac{vh}{Gt} + 0.75he_n + d_a\frac{h}{b}$$

Note that the 3-term deflection equation provided in SDPWS (Equation 4.3-1) may also be used but the deflection calculations must be consistent throughout design.

The wall deflection assumption (Figure 3) is that the total deflection of the FTAO shear wall is equivalent to the average of the deflection of each wall pier in both the positive and negative directions. The wall pier heights also vary depending on the deflection direction and amount of sheathing below the openings. For example, in Figure 3, positive deflection of wall pier 1 (δ1+) is determined using the height measured from the bottom of the opening to the top of the wall due to the resistance of the wall sheathing below the opening. Negative deflection of wall pier 1 (δ1-), is determined using the full wall height.

$$\Delta = \text{average } (\delta 1+, \delta 2+, \delta 3+, \delta 1-, \delta 2-, \delta 3-)$$

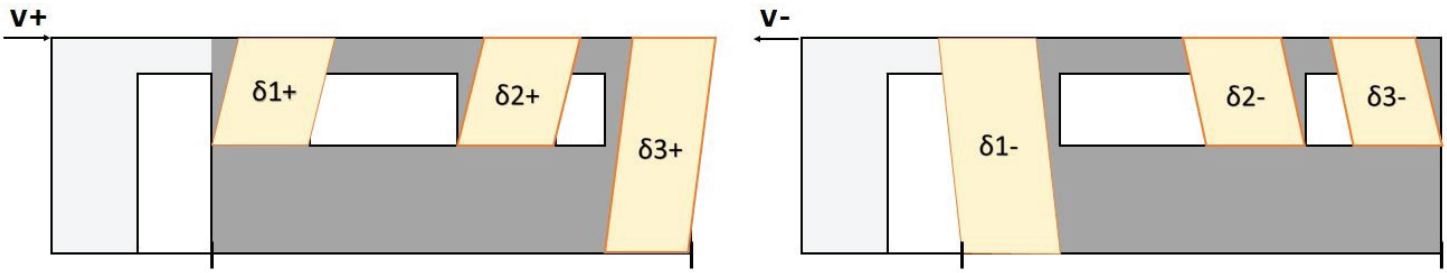

Figure 3: FTAO deflection illustration

continued on next page

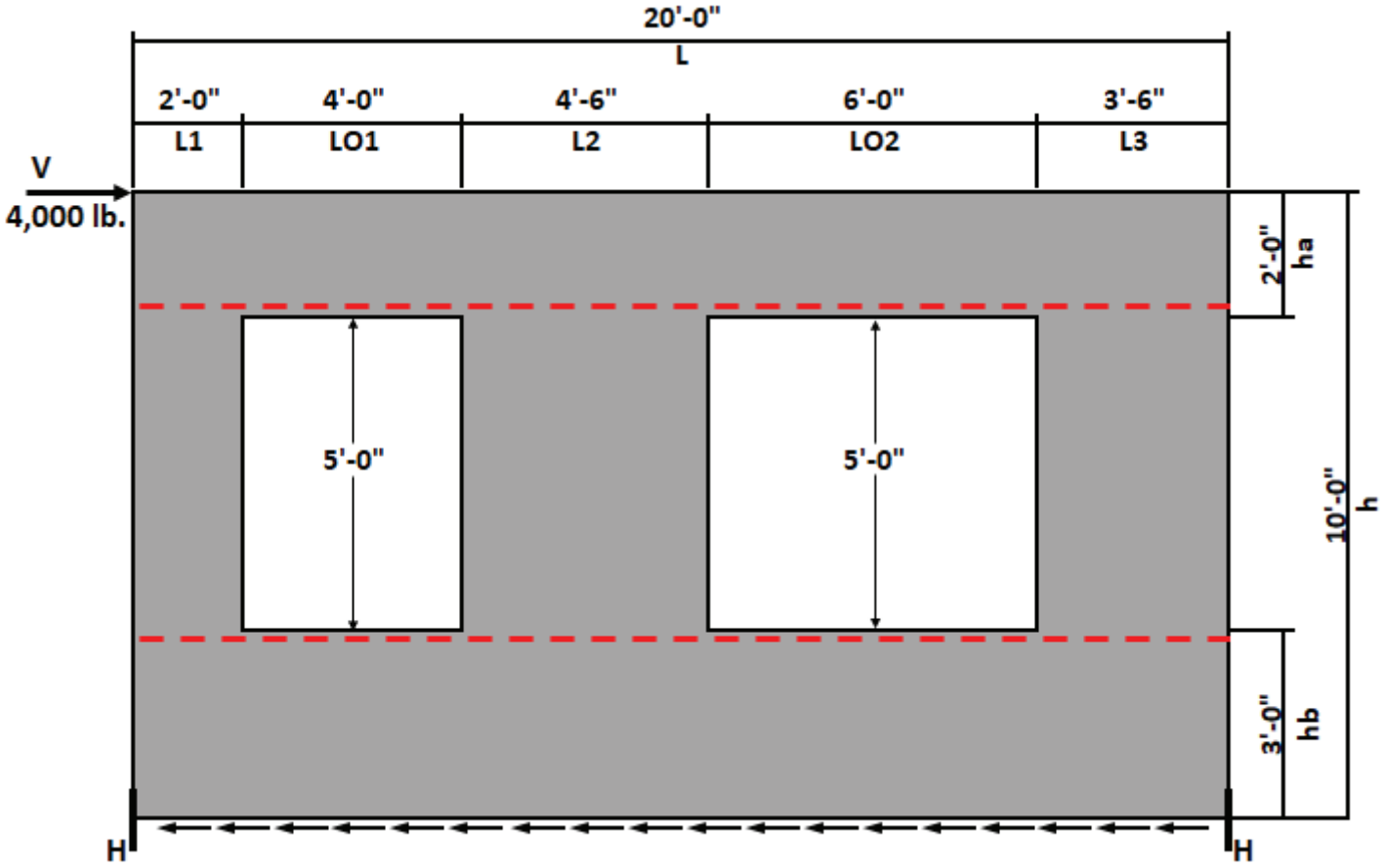

Figure 4: Design Example Illustration

FTAO Design Example

Historically, FTAO design examples have been completed showing symmetric wall pier widths and a single opening in the wall system. Figure 4 illustrates the benefits of FTAO for walls with multiple openings and asymmetric wall pier widths.

Given a 20-foot-long wall that is 10 feet tall with a 4,000 pound shear force applied to the top of the wall, use the FTAO method to calculate hold-down forces, required strap forces, and required wall sheathing capacity.

Begin by calculating the hold-down forces at each end of the shear wall:

1. H = (V*h)/L
   = ((4,000 lb)(10 ft))/(20 ft)
   = 2,000 lb

   The selected hold-downs must have a minimum capacity of 2,000 pounds.

To attain the corner forces, both the unit shear and boundary forces above and below the openings must be determined.

2. Unit Shear Above and Below Openings:
   va = vb = H/(ha + hb)
   = 2,000 lb/(2 ft + 3 ft)
   = 400 plf
3. Total boundary force above and below the openings:
   O_1 = (va)(LO1)
   = (400 plf)(4 ft)
   = 1,600 lb
   O_2 = (va)(LO2)
   = (400 plf)(6 ft)
   = 2,400 lb

continued on next page

Calculate the corner forces at each opening to determine the maximum strap force required:

4. $F_1 = ((O_1)(L1))/(L1 + L2)$
   $= ((1{,}600 \text{ lb})(2 \text{ ft}))/(2 \text{ ft} + 4.5 \text{ ft})$
   $= 492 \text{ lb}$
   $F_2 = ((O_1)(L2))/(L1 + L2)$
   $= ((1{,}600 \text{ lb})(4.5 \text{ ft}))/(2 \text{ ft} + 4.5 \text{ ft})$
   $= 1{,}108 \text{ lb}$
   $F_3 = ((O_2)(L2))/(L2+L3)$
   $= ((2{,}400 \text{ lb})(4.5 \text{ ft}))/(4.5 \text{ ft} + 3.5 \text{ ft})$
   $= 1{,}350 \text{ lb}$
   $F_4 = ((O_2)(L3))/(L2 + L3)$
   $= ((2{,}400 \text{ lb})(3.5 \text{ ft}))/(4.5 \text{ ft} + 3.5 \text{ ft})$
   $= 1{,}050 \text{ lb}$

The selected strapping to be placed above and below the openings must have a minimum tension capacity of 1,350 pounds.

To calculate the unit shear beside the openings and to determine our wall sheathing requirement, the tributary width of each internal shear line must be determined.

5. $T_1 = ((L1)(LO1))/(L1 + L2)$
   $= ((2 \text{ ft})(4 \text{ ft}))/(2 \text{ ft} + 4.5 \text{ ft})$
   $= 1.23 \text{ ft}$
   $T_2 = ((L2)(LO1))/(L1 + L2)$
   $= ((4.5 \text{ ft})(4 \text{ ft}))/(2 \text{ ft} + 4.5 \text{ ft})$
   $= 2.77 \text{ ft}$
   $T_3 = ((L2)(LO2))/(L2 + L3)$
   $= ((4.5 \text{ ft})(6 \text{ ft}))/(4.5 \text{ ft} + 3.5 \text{ ft})$
   $= 3.38 \text{ ft}$
   $T_4 = ((L3)(LO2))/(L2 + L3)$
   $= ((3.5 \text{ ft})(6 \text{ ft}))/(4.5 \text{ ft} + 3.5 \text{ ft})$
   $= 2.63 \text{ ft}$

Using the tributary width to the internal shear lines, the maximum unit shear beside the openings can be calculated to determine the required wall sheathing capacity.

6. $V_1 = ((V/L)(L1 + T_1))/L1$
   $= ((4{,}000 \text{ lb}/20 \text{ ft})(2 \text{ ft} + 1.23 \text{ ft}))/(2 \text{ ft})$
   $= 323 \text{ plf}$
   $V_2 = ((V/L)(T_2 + L2 + T_3)/L2$
   $= ((4{,}000 \text{ lb}/20 \text{ ft})(2.77 \text{ ft} + 4.5 \text{ ft} + 3.38 \text{ ft}))/(4.5 \text{ ft})$
   $= 473 \text{ plf}$
   $V_3 = ((V/L)(T_4 + L3)/L3$
   $= ((4{,}000 \text{ lb}/20 \text{ ft})(2.63 \text{ ft} + 3.5 \text{ ft}))/(3.5 \text{ ft})$
   $= 350 \text{ plf}$

The selected wall sheathing must have a minimum shear capacity of 473 plf.

Note that as a calculation verification the sum of the unit shears multiplied by the length of the adjacent wall pier should be equal to the initial shear force:

$(V_1)(L1) + (V_2)(L2) + (V_3)(L3) = V$
$(323 \text{ plf})(2 \text{ ft}) + (473 \text{ plf})(4.5 \text{ ft}) + (350 \text{ plf})(3.5 \text{ ft}) = 4{,}000 \text{ lb}$ This checks out.

To verify the calculations, the final design assumption must be met. The sum of the shear-line forces at the outside lines must be equal to the hold-down force and the sum of each interior shear line must be equal to zero. To perform this verification the corner force resistance and corner zone unit shears must be determined.

The corner force resistance, R, for each pier is determined by multiplying the unit shear in each wall pier by the corresponding wall pier length:

7. $R_1 = (V_1)(L1)$
   $= (323 \text{ plf})(2 \text{ ft})$
   $= 646 \text{ lb}$
   $R_2 = (V_2)(L2)$
   $= (473 \text{ plf})(4.5 \text{ ft})$
   $= 2{,}129 \text{ lb}$
   $R_3 = (V_3)(L3)$
   $= (350 \text{ plf})(3.5 \text{ ft})$
   $= 1{,}225 \text{ lb}$

continued on next page

To calculate the corner force unit shear in each wall pier first the resultant shear force in the corner zone must be determined, then divided by the corresponding wall pier length:

8. R1-F1 = 646 lb – 492 lb = 154 lb
   R2-F2-F3 = 2,129 lb – 1,108 lb – 1,350 lb = -329 lb
   R3-F4 = 1,225 lb – 1,050 lb = 175 lb
9. $vc_1 = (R_1\text{-}F_1)/L1$
   = (154 lb)/2 ft
   = 77 plf
   $vc_2 = (R_2\text{-}F_2\text{-}F_3)/L2$
   = (-329 lb)/4.5 ft
   = -73 plf
   $vc_3 = (R_3 - F_4)/L3$
   = (175 lb)/3.5 ft
   = 50 plf

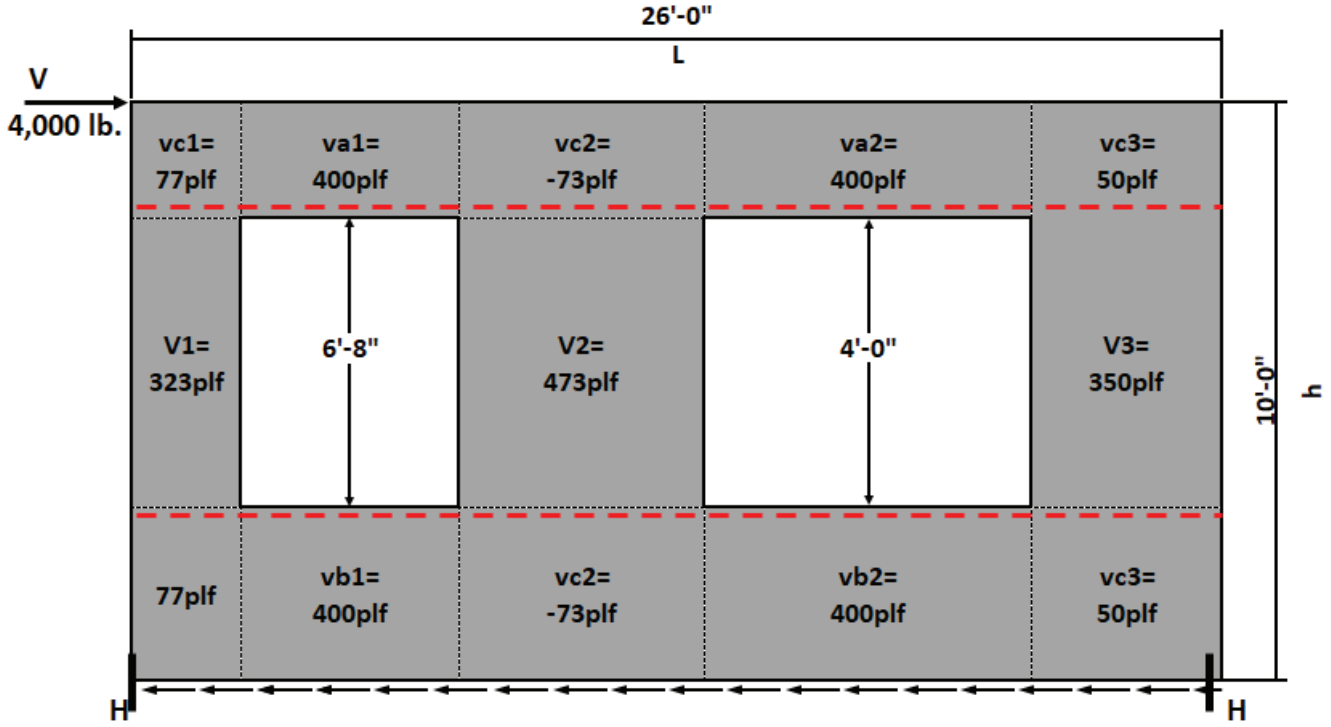

Figure 5: Wall Force Diagram Illustration

Performing a design check by summing the forces at each shear line will complete the analysis:

10. Line 1: $(va_1)(ha + hb) + (V_1)(ho) = H$?
    (77 plf)(2 ft + 3 ft) + (323 plf)(5 ft) = 2,000 lb
    Line 2: $(va)(ha + hb) - (va_1)(ha + hb) - (V_1)(ho) = 0$?
    (400 plf)(2 ft + 3 ft) - (77 plf)(2 ft + 3 ft) - (323 plf)(5 ft) = 0
    Line 3: $(va_2)(ha + hb) + (V_2)(ho) - (va)(ha + hb) = 0$?
    (-73 plf)(2 ft + 3 ft) + (473 plf)(5 ft) - (400 plf)(2 ft + 3 ft) = 0
    Line 4 = Line 3
    Line 5: $(va)(ha + hb) - (va_3)(ha + hb) - (V_3)(ho) = 0$?
    (400 plf)(2 ft + 3 ft) - (50 plf)(2 ft + 3 ft) - (350 plf)(5 ft) = 0
    Line 6: $(va_3)(ha + hb) + (V_3)(ho) = H$?
    (50 plf)(2 ft + 3 ft) + (350 plf)(5 ft) = 2,000 lb

continued on next page

Using the 4-term deflection equation (Figure 3), overall wall deflection is calculated by determining the average of the positive and negative deflection values for each pier (Figure 4). Assuming a maximum hold-down capacity of 2,500 pounds, nail slip of 0.125 inches, and an APA Rated Sheathing 15/32" performance category with 8d nails at 4" on center:

11. Δ = average ($\delta 1+, \delta 2+, \delta 3+, \delta 1-, \delta 2-, \delta 3-$)
= average (1.393,0.692,0.508,0.708,0.692,0.963) (in)
= 0.826 in.

APA has automated the calculation process in the previous example with the creation of an FTAO spreadsheet (https://www.apawood.org/designerscircle-ftao). The spreadsheet is based on the tested methodology and provides the engineer with the required hold-down forces, tension strap forces, wall sheathing capacity, and automatically completes the design check in step 9. The spreadsheet also provides shear wall deflection calculations for the 3- and 4-term deflection equation options.

Conclusion

With the introduction of a new method for estimating the overall wall deflection and tested verification for the accuracy of force transfer around openings (FTAO) shear walls, designers can be confident in having another valuable tool to apply when designing the lateral resisting system for wood buildings. The FTAO method helps expand the boundaries of building design with wood-framed walls, utilizing the full shear wall geometry to help increase the design flexibility and potentially reduce the economic impact of the lateral resisting system.

Jared S. Hensley, P.E. holds a Bachelor of Science in Architectural Engineering with an emphasis in structural design from the University of Wyoming. An expert in residential and commercial design with engineered wood products, Jared is currently the Director of Engineering at Rosboro. All research and testing for the development of this methodology/article was completed under the direction of APA - The Engineered Wood Association. For technical questions please contact the APA Product Support Help Desk at helpdesk@apawood.org or 253-620-7400.

Full-Scale Shake Table Testing of a Two-Story Mass Timber Building with Resilient Rocking Wall Lateral Systems

Dr. Shiling Pei, P.E., Hans-Erik Blomgren, P.E., S.E., P.Eng., Struct.Eng., Dr. Andre Barbosa, Dr. John W. van de Lindt, Eric McDonnell, P.E., Dr. Jeff Berman, and Dr. James Dolan, P.E.

Introduction

In July 2017, a full-scale two-story mass timber building was subjected to twenty-seven seismic tests on the world's largest outdoor shake table at University of California, San Diego (UCSD). This test program marked the beginning of a collaborative research project (NHERI Tallwood Project) funded by the National Science Foundation with the intention to develop resilience-based seismic design methodology for tall wood buildings. The two-story mass timber system with two types of cross laminated timber (CLT) rocking walls is the first of its kind tested on a shake table at full scale world-wide. This series of tests provided a benchmark data-set for seismic response of this innovative building system, which is used to guide the subsequent research and development of seismically resilient tall wood buildings. The motivation, implementation, and summary results of this test program are presented in this article.

Background and Motivation

After the introduction of Cross Laminated Timber (CLT, see Figure 1) into the U.S. in the early 2000's, there is an on-going effort to expand the wood building market beyond low-rise construction using mass timber construction, namely buildings using a combination of CLT panels and heavy timber beam and column elements. With a significant portion of the U.S. population residing in regions with moderate to high seismicity, mass timber buildings in these regions must demonstrate that they can satisfy or even exceed building code life safety requirements. This condition provided the motivation of the NHERI Tallwood Project, which has the vision to develop tall mass timber buildings that can survive large earthquakes with minimal repairable damage.

The performance of CLT buildings under seismic loading has been studied by researchers around the world since the early 2000's. A number of previous research projects on CLT systems focused on platform style CLT construction in which panelized CLT walls served as both the gravity system and the lateral system. Component and system level tests for platform CLT buildings, including a 7-story CLT building shake table test (Ceccotti et al. 2013), were conducted by researchers around the world (Pei et al. 2014). These earlier research revealed that the rigidity of the platform construction style makes it difficult to survive large earthquakes without damage. This is because rigidly connected CLT panels in a platform style building needs to dissipate energy and develop ductile response through connection damage. Such systems will be able to satisfy life-safety requirement of the code, but will require significant effort to repair after large earthquakes.

Figure 1: Cross Laminated Timber (CLT) panel

continued on next page

Different from these past efforts, this test program investigated a balloon framed mass timber system combining CLT rocking wall lateral systems with CLT diaphragm and glulam gravity frames. There are two different CLT rocking wall systems investigated, namely a post-tensioned rocking wall system studied in Phase I and a repairable rocking wall without post-tension tested in Phase II. Firstly, post-tensioned wood rocking wall systems were initially studied by researchers in New Zealand (Iqbal et al. 2015, Buchanan et al. 2008) and used in real building projects (Palermo et al. 2012). A prototype LVL panel rocking wall was later introduced to North American by FPInnovations. Prior to this shake table test, a reversed cyclic load testing of post-tensioned CLT rocking walls was conducted by the research team (Ganey et al. 2017) to collect load-resistance data of this lateral system. Results from the component tests indicated that post-tensioned CLT rocking wall can provide very good ductility while limit non-recoverable damage at large drift levels. The researchers hypothesize that this lateral system can be used in a mass timber building to significantly reduce earthquake-induced damage. In addition to the post-tensioned rocking wall system, industry collaborator Katerra also conceptualized a rocking wall option (referred herein as Katerra wall) without post-tensioning by focusing on reparability of the building. This rocking wall system eliminated post-tensioning process to enable even faster installation, while uses replaceable energy dissipation components that are designed to get damaged during large earthquakes. The hypothesis on the Katerra wall performance is that it will not need repair during service level earthquakes, but will be quickly repairable in larger events.

The most convincing way to validate these hypothesis is to build and test a full-scale mass timber building using the proposed systems on a shake table. Although the intention of the project is to use these systems in tall building configurations, a two-story building was decided by the research team as a reasonable starting point, considering the novelty of the system and also the resources available for testing. The test program was divided into two phases, namely Phase I with the post-tensioned CLT rocking wall, and Phase II with the reparable rocking wall from Katerra. The research team is intended to use the knowledge gained through this test to eventually design and test a full-scale ten-story mass timber building in 2020.

Test Building: Design and Construction

The scope of the test program was driven by the key questions it was designed to answer, which mainly include:

- Can we achieve seismically resilient performance in an open-floor plan wood building through use of CLT rocking walls?
- How to design the gravity frame system so it can work compatibly with the rocking wall system without damage?
- How to safely and effectively transfer lateral force between the building diaphragms and the balloon-framed rocking walls?
- How to design CLT diaphragms to eliminate or reduce its damage in large earthquakes?

The exact dimensions of the test specimen was determined based on the desired diaphragm aspect ratio, the need for an open floor plan, and the limitations of the shake table. This led to a design features a 6.7m (22 ft) tall test building (3.7m (12 ft) at first floor, 3m (10 ft) at the second floor) with a 17.7x6.1m (58 x 20 ft) floor plan as shown in Figure 2. The specimen has a very open floor plan and relatively realistic diaphragm aspect ratio in the direction of the shaking (the UCSD shake table is a uniaxial table that shakes only in one direction).

continued on next page

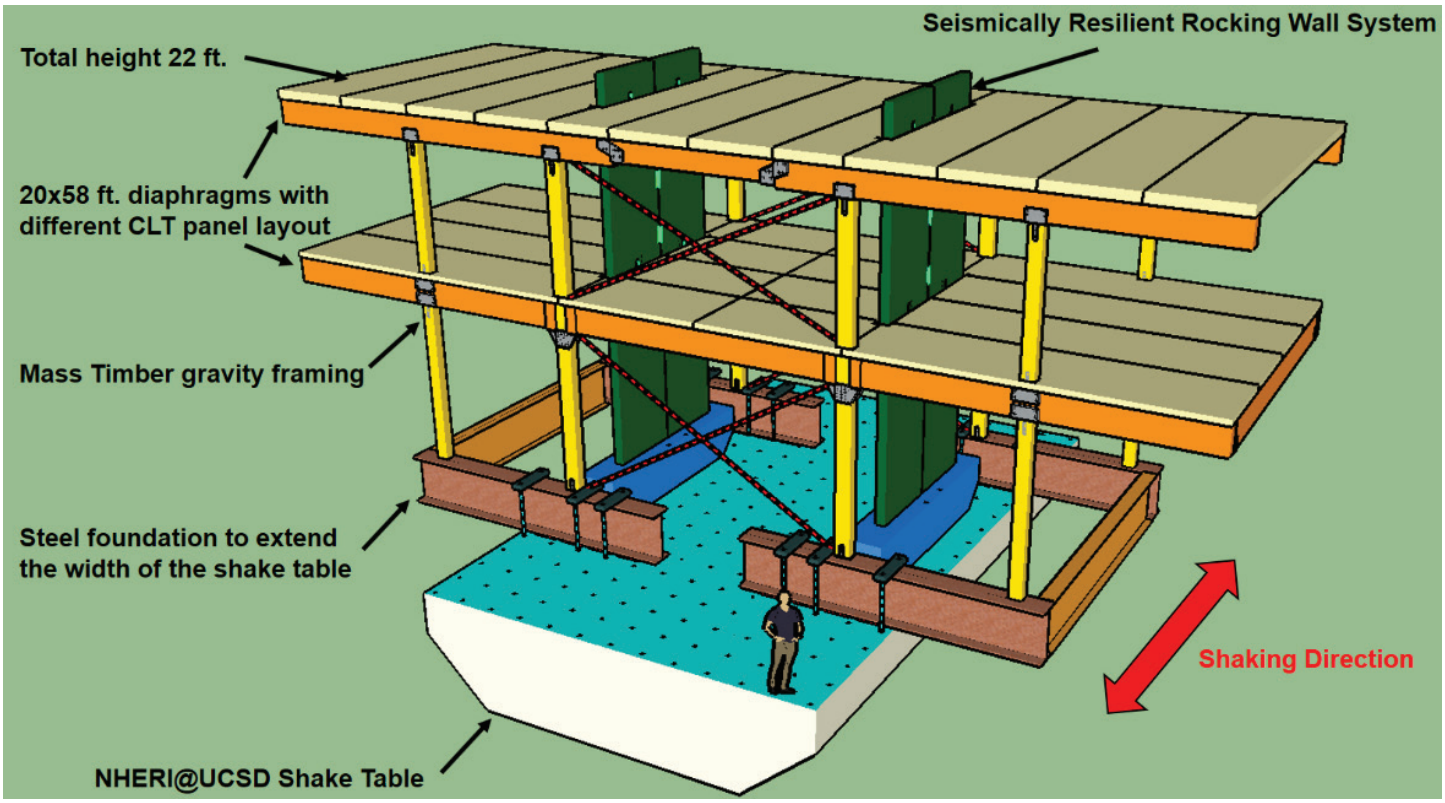

Figure 2: Two-story mass timber test building

Two diaphragm designs with different CLT panel and glulam beam grid arrangements were investigated including one with composite concrete topping and the other with CLT panels only. The design of the un-topped CLT floor diaphragm and sizing of the chord connectors (metal straps fastened to the CLT using self-tapping screws) over panel splices were determined in accordance with principles of mechanics using design values of fastener and member strength (values from the US 2015 National Design Specification (NDS) for Wood Construction, manufacturer specifications, or testing). The design of concrete-CLT composite roof diaphragm was conducted based on earlier testing of similar composite floors at Oregon State University (Higgins et al. 2017, Johnson 2017) and with basic principles of composite members.

In order to accommodate the large inter-story drift, the gravity framing connections were designed to rock at the beam-to-column interface. Additionally, a combination of platform and balloon framed columns (i.e., discontinuous and continuous at the first floor) were used to investigate the feasibility of connections for both framing methods. For platform framed column-beam joints, modified standard Simpson Strong-Tie column caps were installed with slotted bolt holes to allow joint rotation. For the balloon framed columns, a custom designed paired beam seating connection was utilized. The connection details were inspired by a design by KPFF Consulting Engineers for the proposed Glenwood CLT Parking Garage project in Springfield, OR and the proposed Framework project (Zimmerman and McDonnell 2018) in Portland, OR. These connections permit shear transfer of diaphragm forces during simultaneous uplift of the CLT rocking walls.

The CLT material used in this study was provided by a U.S. CLT manufacture (DR. Johnson Lumber) certified as Grade V1 based on APA standard PRG320 (APA, 2011) for CLT panels. The floor CLT was 3-ply panel and the roof and rocking wall

continued on next page

panels were 5-ply. The glulam beams and columns were provided by the same manufacturer with a minimum of 24F-V4 grade for beams and L2 grade for columns.

Rocking Wall Design Considerations

Both test phases included two sets of coupled CLT rocking walls designed based on a combination of force-based and displacement-based criteria. For the post-tensioned rocking walls, CLT panels were coupled using U-shaped flexural steel plate (UFP) energy dissipaters. Similar energy dissipaters were used in concrete rocking wall systems (Priestley et al. 1999, Johnston et al. 2014), as well as the CLT rocking walls tested by Ganey et al. 2017. The Katerra wall panels were coupled using a custom designed steel plate with cutting patterns specifically chosen to achieve a desired shear behavior. The post-tensioned wall dimensions and initial PT force were selected to achieve decompression limit state under the seismic demands computed per ASCE 7-10 (ASCE 2010) for a Class B soil site in San Francisco with an assumed seismic force reduction factor, *R*, of 6, the approximate period per ASCE 7-10. Additional limit states such as crushing of the wood panel and yielding of the post-tensioned steel bar were designed to be reached at different lateral drift levels. A trial-and-error performance-based design with nonlinear model validation was adopted for the design of the Katerra wall system following a predetermined set of performance criteria including: 1) No damage under service level earthquake (approximately 50% probability of exceedance in 50 years); 2) Drift not exceeding 2.5% under Design Basis Earthquake (DBE) with easily repairable damage; and 3) Drift not exceeding 3.75% under Maximum Considered Earthquake (MCE) with heavy but repairable damage. The damage to the Katerra wall system should only occur at the replaceable components for all tests. Photos of the constructed rocking walls are shown in Figure 3 below.

(a) (b)

Figure 3: Photos of two different types of rocking walls (a) Post-tensioned wall (b) Katerra wall

continued on next page

Construction process

The construction of the test building was contracted to Seagate Structures Ltd. American. There were a total of two carpenters on site during the construction process. The UCSD site crew (two persons) helped to operate the crane. The construction of the wood gravity frame only took four days. The preparing and pouring of the concrete composite layer was performed by a different concrete contractor after the wood frame was completed. After the concrete hardened, the CLT rocking walls were inserted into the building and connected to the diaphragm and the foundation. During this process, additional steel trench plates were also placed on the floor and the roof in order to bring the total seismic mass to the desired levels (total mass of 321 kg/m^2 (64 pound per-square foot, psf) for the floor and 386kg/m2 (79 psf) for the roof). The last step of construction is the post-tensioning of the rocking wall. Because the needed post-tension force level is relatively low, the post-tensioning was achieved by tightening the nuts manually while monitoring the tension forces using load cells. The building with post-tensioned rocking wall system was tested first (Phase I), followed by the removal of the post-tensioned rocking wall and the installation of the Katerra wall system (for Phase II). Key steps in the construction process were illustrated in Figure 4. The completed building was shown in Figure 5.

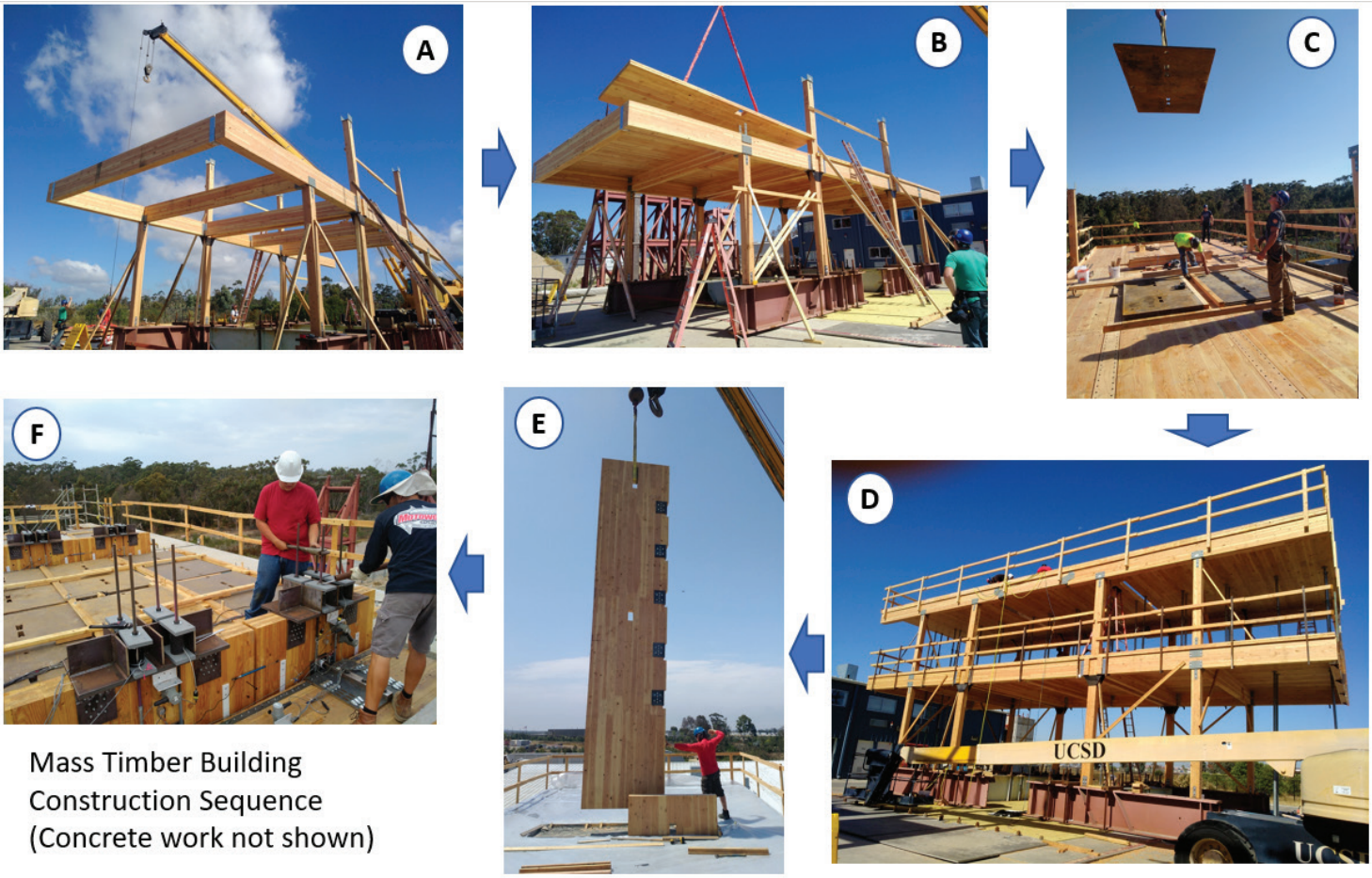

Figure 4: Construction process of the test building (only showing wood construction) (Pei et al. 2018)

continued on next page

Figure 5: The test building completed with post-tension rocking walls

Testing program

Earthquake ground motions recorded from historical earthquakes were used in the testing program, including ground motions from the Northridge and Loma Prieta earthquakes. These ground motions were scaled to represent different hazard levels corresponding to two locations on the west coast, namely San Francisco CA and Seattle WA. There are three hazard levels for each location, namely the service level earthquake (SLE), design basis earthquake (DBE), and maximum considered earthquake (MCE).

All shake table tests conducted in both Phase I and II are listed in Table 1, together with the maximum roof drift (calculated as the roof displacement divided by the building height). Because it is not possible for the shake table to completely reproduce the ground motion inputs (this is common for large shake tables), the peak ground acceleration (PGA) and spectral acceleration (Sa) values listed in the Table were obtained from the measured actual acceleration time history from the shake table. The spectral acceleration values were given at 0.9 second natural period because that is roughly close to the measured natural period of the building. The response spectrum of the ground motions at different levels were plotted in Figure 6.

continued on next page

Table 1. Ground motion used in the test and maximum roof drifts

ID	Ground Motion	Hazard level*	PGA (g)	Sa @ 0.9 sec (g)	Maximum roof drift (%)
1-1	Loma Prieta	SLE (SF)	0.17	0.16	0.78
1-2	Loma Prieta	SLE (SF)	0.19	0.16	0.81
1-3	Northridge	SLE(SF)	0.19	0.18	0.50
1-4	Superstition Hill	SLE(SF)	0.13	0.12	0.39
1-5	Northridge	DBE(SF)	0.54	0.70	2.63
1-6	Northridge Repeated	Original	0.56	0.76	2.54
1-7	Imperial Valley	SLE(SF)	0.14	0.22	0.83
1-8	Northridge Repeated	Original	0.55	0.76	2.63
1-9	Loma Prieta	DBE(SF)	0.54	0.50	1.65
1-10	Superstition Hill	DBE(SF)	0.48	0.43	2.12
1-11	Loma Prieta	MCE (SF)	0.66	0.58	1.93
1-12	Northridge	MCE(SF)	0.76	0.92	3.27
1-13	Superstition Hill	MCE(SF)	0.68	0.63	3.28
1-14	Northridge	MCE x 1.2(SF)	0.89	1.12	5.07
2-1	Superstition Hill	SLE (SEA)	0.15	0.13	0.49
2-2	Imperial Valley	SLE(SF)	0.19	0.33	0.90
2-3	Northridge	SLE(SEA)	0.11	0.14	0.54
2-4	Loma Prieta	SLE(SEA)	0.16	0.14	0.47
2-5	Superstition Hill	DBE(SEA)	0.46	0.47	1.49
2-6	Imperial Valley	DBE(SEA)	0.42	0.77	1.50
2-7	Northridge	DBE(SEA)	0.13	0.15	0.51
2-8	Imperial Valley	DBE(SEA)	0.43	0.79	1.52
2-9	Northridge	DBE(SF)	0.45	0.61	2.55
2-10	Northridge	MCE(SF)	0.69	0.93	3.39
2-11	Loma Prieta	SLE(SEA)	0.15	0.15	0.49
2-12	Imperial Valley	MCE x 1.2(SF)	0.84	1.56	2.99
2-13	Northridge	MCE x 1.2(SF)	0.82	1.13	3.83

** Scaling of the ground motion was based on seismic hazard near San Francisco (SF) or Seattle (SEA)*

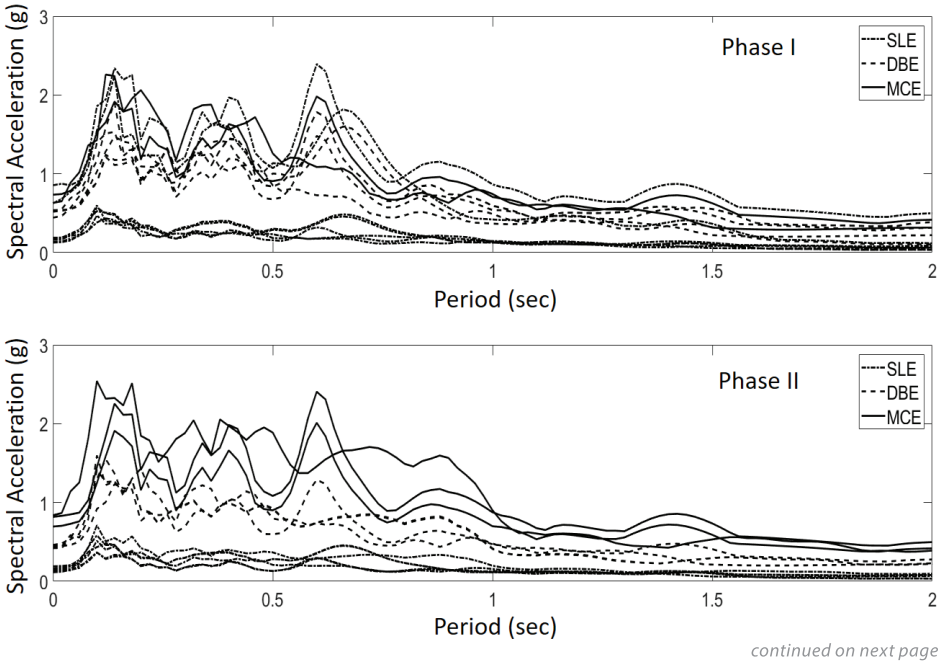

Figure 6: Response spectrum of the ground motions used in the tests

continued on next page

Test Results

The most important objective of the test program is to validate the resilience of the mass timber system design. The research team conducted very detailed damage inspection on all seismic tests at or above the DBE level. Although the lateral system of the test building was changed between the testing Phases, the gravity frame and diaphragm system remained the same and withstood a total of 27 earthquake excitations without notable damage. The diaphragm behaved elastically and no damage was observed either.

As it is listed in Table 1, the post-tensioned rocking wall system was tested to achieve a maximum of over 5% inter-story drift. Some post-tension loss was observed in MCE level tests, which indicated yielding of the post-tension bars at some locations. This damage was easily repaired through re-tensioning of the post-tension rods. The post-tensioned rocking wall was able to keep the building re-centered even with the post-tension losses (only a small portion of the post-tension rods yielded). The building residual drift was under 0.5% for all tests conducted in Phase I. The only visible damage was found at the bottom corners of the rocking wall panels. The damage was mostly cosmetic including splitting of the outside wood fiber and slight deformation of the corner. After the test was completed and the rocking walls were taken out of the building, slight compression deformation was observed at the rocking wall toe. All the damage (see Figure 7) did not affect the performance of the system thus required no repair. The resilient performance target was verified for the post-tensioned rocking wall system.

Slight compression deformation at the rocking wall corner

Chipping of wood at the rocking wall corner

Figure 7: Observed damage at the tow location of the post-tensioned rocking wall (Pei et al. 2018)

continued on next page

The Katerra wall system has replaceable components that were designed to be damaged and replaced under DBE and MCE ground motions. This as-designed performance was validated by the test results. Figure 8 shows the damaged crushing block and the yielded inter-panel connectors. Note these components were not damaged during the SLE level shakes. The residual drifts observed during the Phase II tests were all under 1%, which enabled quick repair by jacking the wall corner and replacing the crushing block/inter-panel connectors.

The test building was instrumented with close to 350 channels of sensors including accelerometers, displacement sensors, strain gauges, and load cells. Detailed analysis and presentation of these measured data can be found in another journal paper by Pei et al. (2018). Some selected results from the data analysis were presented here. Figure 9 shows the maximum global displacement responses at the floor and roof level for two test phases, together with select example time history plots from selected tests at different intensity levels. The maximum building base shear (calculated indirectly based on acceleration record and building seismic mass) is presented for both testing phases in Figure 10. As a reminder, the total building design weight is about 75 metric ton, which translate to approximately 730kN in gravity. The example global hysteresis loops are also plotted from representative tests. The acceleration records used in generating these base shear values and hysteresis loops were original recordings that are not filtered.

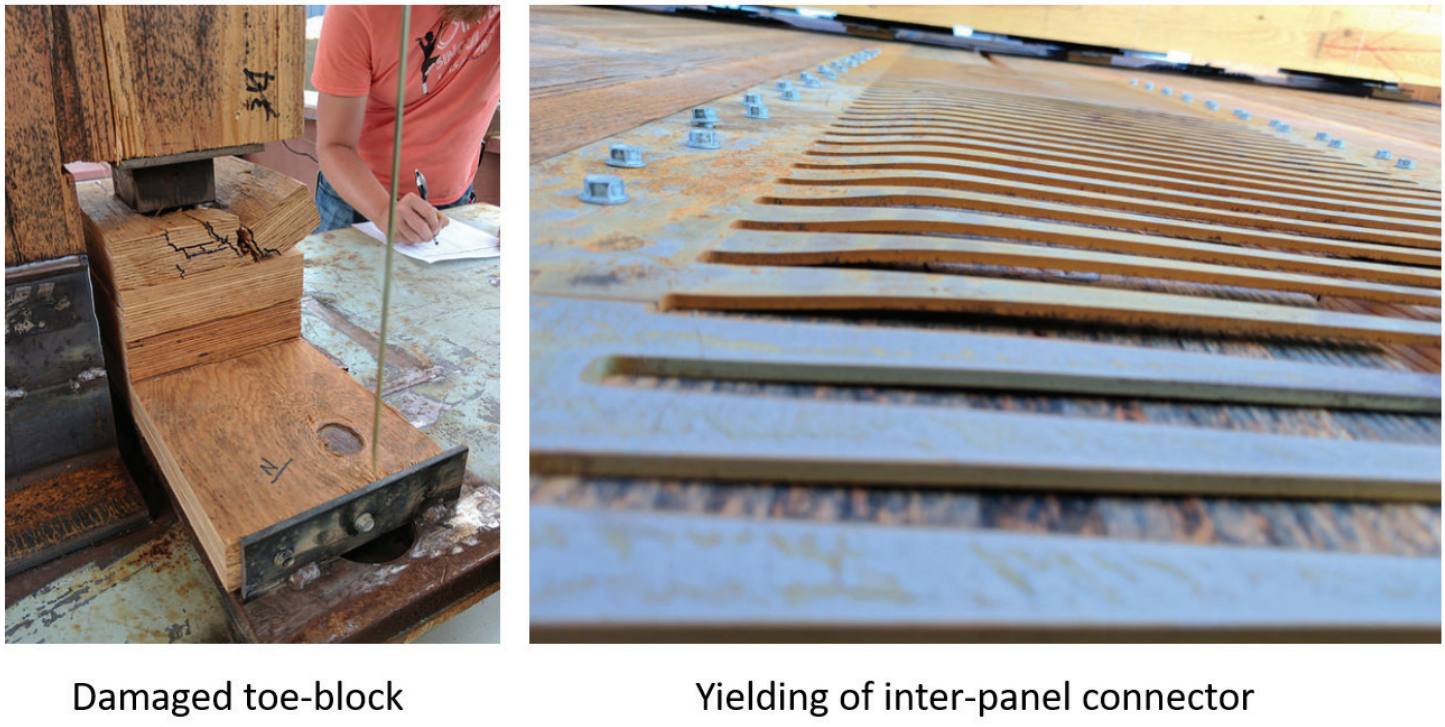

Figure 8: Damage to the repairable components of the Katerra wall

continued on next page

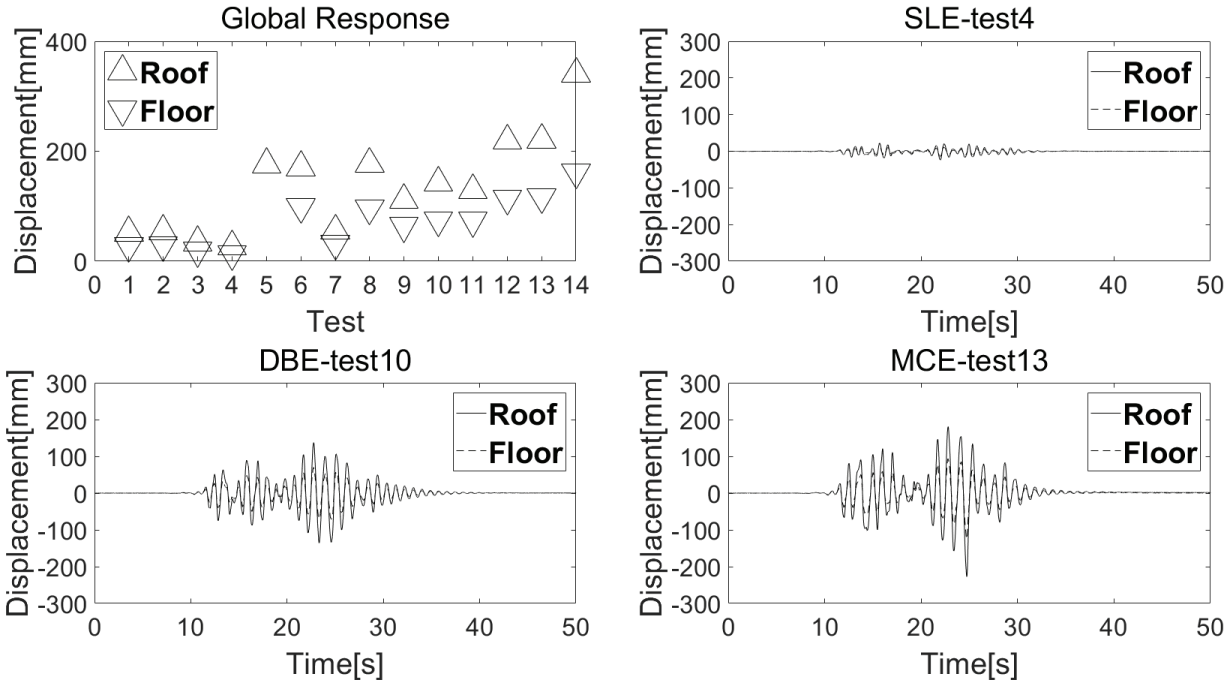

(a)

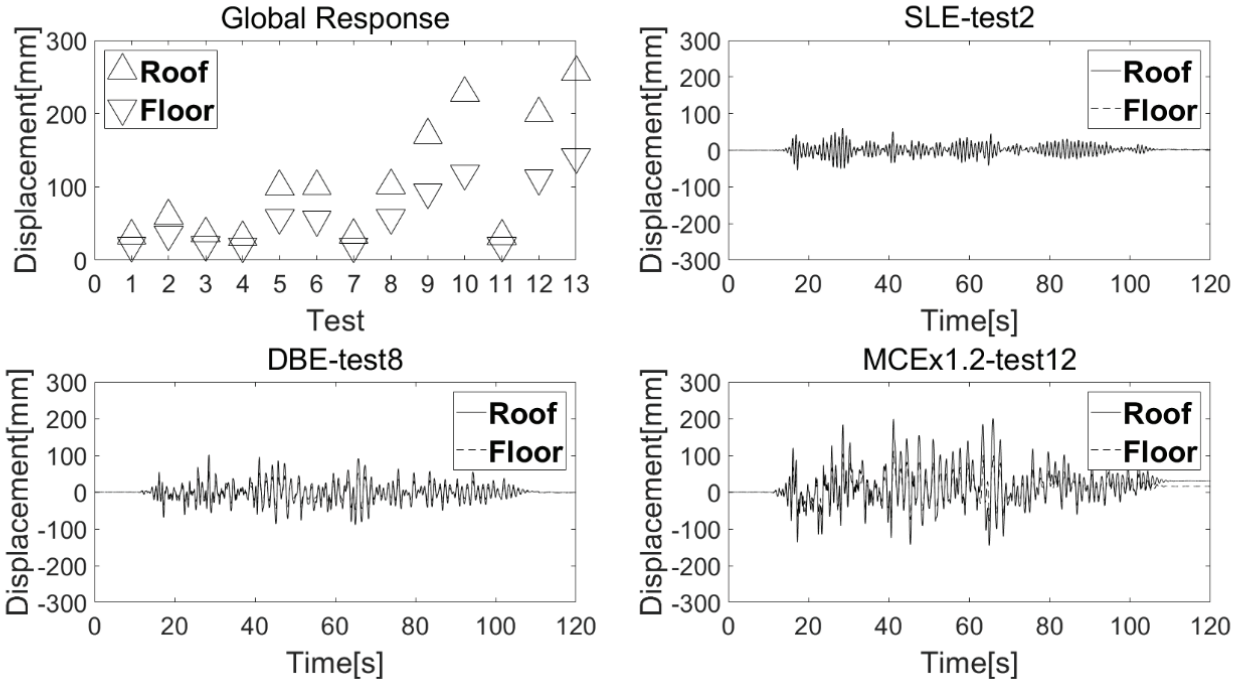

(b)

Figure 9: Maximum building responses and example time history plots for (a) Phase I (b) Phase II

continued on next page

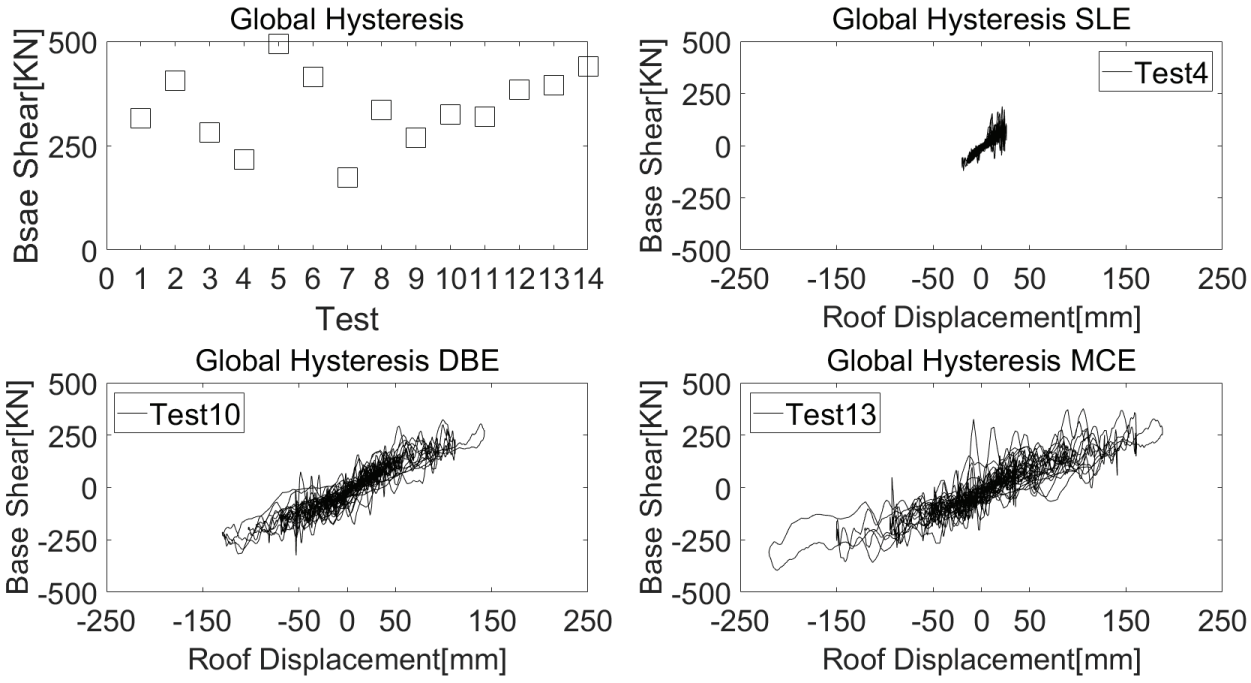

(a)

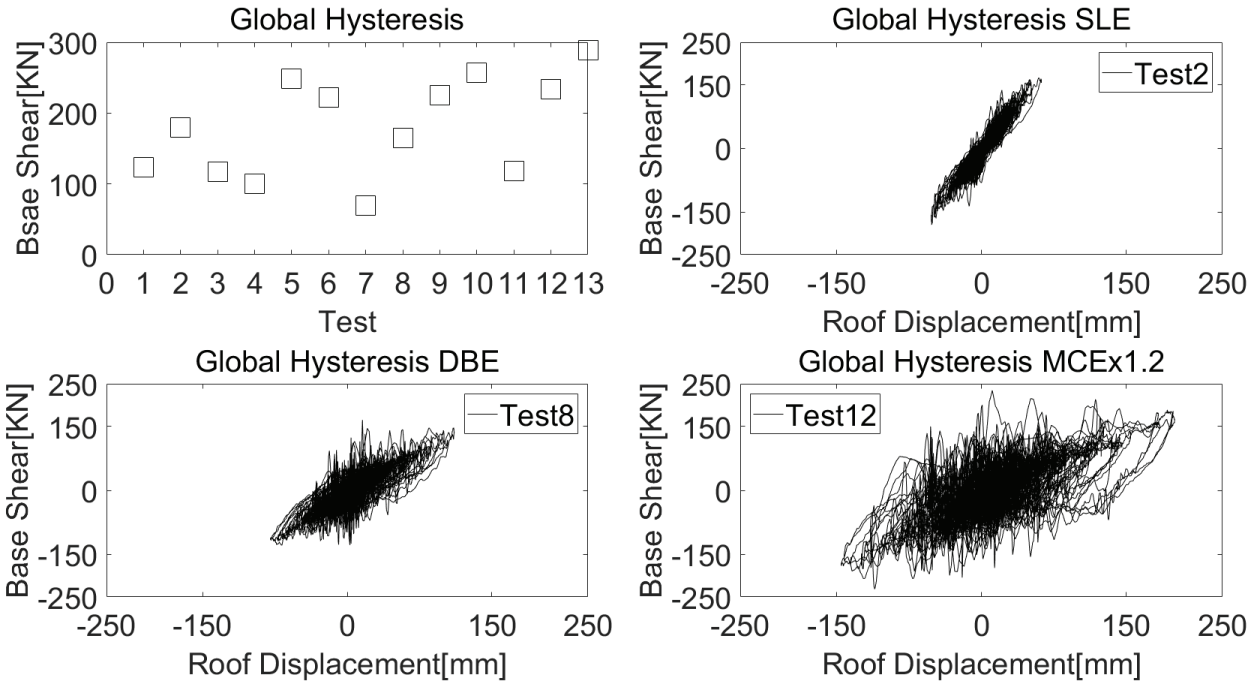

(b)

Figure 10: Maximum building base shear and example global hysteresis plots for (a) Phase I (b) Phase II

continued on next page

Conclusions and Future Work

From the analysis of test results and observed damage from the large earthquakes, it can be concluded that it is possible to combine a CLT rocking wall system with a heavy timber gravity system to achieve resilient performance under large earthquakes at DBE and MCE intensity levels. An open-floor plan mass timber building can be structurally resilient under multiple earthquake excitations. This resilient performance is significantly better than typical seismic performance observed in most existing building lateral systems under similar levels of seismic excitation. In addition, this design enables very fast construction by a small on-site crew.

By using simple connection details and connectors readily available on the market, CLT diaphragms can be designed to adequately transfer lateral forces under large earthquakes. The shear transfer detail between the diaphragm and rocking wall performed very well during large earthquakes. Over-strength for such details is recommended in their design in order to keep them elastic under earthquake loading. The gravity connection details used in this test program can tolerate up to 5% inter-story drift without inducing damage or losing stability.

While having the resilience performance described above, the mass timber test building had a relatively low stiffness compared to a typical two-story building. When applying the same lateral system to a tall building design, this lack of initial stiffness can become a challenge in limiting seismic or even wind-induced deformations and vibrations. In addition, fire performance of tall wood buildings is not well-understood by the engineering community and the public at this point, leaving a significant barrier for developing tall wood buildings. Building on the foundation of the knowledge obtained from the two-story test, NHERI TallWood research team is planning on the design and testing of a full-scale 10-story mass timber building with resilient performance in 2020.

Acknowledgement

The NHERI TallWood project is supported by the National Science Foundation through a number of collaborative awards including: CMMI 1636164, CMMI 1634204, CMMI 1635363, CMMI 1635227, CMMI 1635156, CMMI 1634628. The use of NHERI experimental facility is supported by the National Science Foundation's Natural Hazards Engineering Research Infrastructure Program. The authors would also like to acknowledge support for the two-story shake table testing program from industry and research partners including: Katerra, Softwood Lumber Board, Simpson Strong-Tie, Forest Products Laboratory, the TallWood Design Institute, DR Johnson Lumber, and the City of Springfield, Oregon. The opinions presented here are solely those of the authors and do not necessarily represent that of the sponsors.

References

American Society of Civil Engineers. (2010) Minimum Design Loads for Buildings and Other Structures, American Society of Civil Engineers, Reston, VA

APA-The Engineered Wood Association. (2011). Standard for Performance-Rated Cross Laminated Timber, ANSI/APA PRG 320. Tacoma, Washington, USA.

Buchanan, Andy, Bruce Deam, Massimo Fragiacomo, Stefano Pampanin, and Alessandro Palermo. (2008) "Multi-storey prestressed timber buildings in New Zealand." Structural Engineering International 18, no. 2: 166-173.

Ceccotti, Ario, Carmen Sandhaas, Minoru Okabe, Motoi Yasumura, Chikahiro Minowa, and Naohito Kawai. (2013) "SOFIE project–3D shaking table test on a seven-storey full-scale cross-laminated timber building." Earthquake Engineering & Structural Dynamics 42, no. 13: 2003-2021.

continued on next page

Ganey, Ryan, Jeffrey Berman, Tugce Akbas, Sara Loftus, J. Daniel Dolan, Richard Sause, James Ricles, Shiling Pei, John van de Lindt, and Hans-Erik Blomgren. "Experimental Investigation of Self-Centering Cross-Laminated Timber Walls." Journal of Structural Engineering 143, no. 10 (2017): 04017135.

Higgins, C., Barbosa, A.R., Blank, C. (2017). "Structural Tests of Composite Concrete-Cross-Laminated Timber Floors." Oregon State University, Corvallis, Oregon, USA.

Iqbal, A., Pampanin, S., Palermo, A., & Buchanan, A. H. (2015). Performance and design of LVL walls coupled with UFP dissipaters. Journal of Earthquake Engineering, 19(3), 383-409.

Johnson, B. (2017). "Timber Tower Research Project – SOM: Physical Testing Report #1, Composite Timber Floor Testing at Oregon State University." Available online at: https://www.som.com/FILE/27750/2017_timber_tower_som_osu_report.pdf (checked 5/8/2018)

Johnston, H., Watson, C., Pampanin, S., & Palermo, A. (2014, August). Shake table testing of an integrated low damage building system. In 2nd European conference in earthquake engineering and seismology, Istanbul (pp. 25-29).

Palermo, A., Sarti, F., Baird, A., Bonardi, D., Dekker, D., & Chung, S. (2012, September). From theory to practice: Design, analysis and construction of dissipative timber rocking post-tensioning wall system for Carterton Events Centre, New Zealand. In Proceedings of the 15th World Conference on Earthquake Engineering, Lisbon, Portugal (pp. 24-28).

Pei, S., Van De Lindt, J.W., Popovski, M., Berman, J.W., Dolan, J.D., Ricles, J., Sause, R., Blomgren, H. and Rammer, D.R., (2014). Cross-laminated timber for seismic regions: Progress and challenges for research and implementation. Journal of Structural Engineering, 142(4), p.E2514001.

Pei S., van de Lindt J.W., Barbosa A., Berman J.W., McDonnell E., Dolan J.D., Blomgren H., Zimmerman R.B., Huang D., Wichman S.(2018) Experimental seismic response of a resilient two-story mass timber building with post-tensioned rocking walls. ASCE Journal of Structural Engineering. Submitted.

Priestley, M. N., Sritharan, S., Conley, J. R., & Pampanin, S. (1999). Preliminary results and conclusions from the PRESSS five-story precast concrete test building. PCI journal, 44(6), 42-67.

Zimmerman, R.B. and McDonnell, E. (2018). "Framework – Innovation in Re-Centering Mass Timber Wall Buildings," Proceedings of the 11th National Conference in Earthquake Engineering, Earthquake Engineering Research Institute, Los Angeles, CA.

Dr. Shiling Pei, P.E.- Associate Professor, Colorado School of Mines, Golden CO 80403, spei@mines.edu

Hans-Erik Blomgren, P.E., S.E., P.Eng., Struct.Eng. - Director of Testing and Characterization, Katerra, Seattle WA

Dr. Andre Barbosa - Assistant Professor, Oregon State University, Corvallis OR

Dr. John W. van de Lindt - Harold H. Short Endowed Chair Professor, Colorado State University, Fort Collins CO

Eric McDonnell, P.E. - Associate, KPFF Consulting Engineers, Portland OR

Dr. Jeff Berman - Professor, University of Washington, Seattle WA

Dr. James Dolan, P.E. - Professor, Washington State University, Pullman WA

Prototyping a Passively Self-Centering Cross-Laminated Timber Rocking Wall System: Analytical and Experimental Investigation

Marco Lo Ricco, P.E., S.E., Dr. Al Ghorbanpoor, P.E., Dr. Shiling Pei, P.E., Doug Rammer, P.E., Marshall Begel, P.E., James Bridwell, M.S., and Reid B. Zimmerman, P.E., S.E.

Abstract:

Cross-Laminated Timber (CLT) garners international interest with increasingly taller wood structures built of robust, rigid panels. For seismic resilience of multistory platform construction, this study prototypes a CLT rocking wall system with an elliptical boundary profile. Curvilinear cuts to the load-bearing edges of a rectangular CLT panel produce smoother lateral response to earthquakes, with gravity-driven passive re-centering ability and reduced crushing damage at wall corners. Stiffness and ductility of the rocking wall can be tuned by proportioning the ellipse profile. Connections between the rocking wall and diaphragm can be designed to transfer shear and influence rocking behavior. This paper presents the design and full scale cyclic testing performance of a prototype CLT rocking wall with two different types of connections. Hysteresis plots of the test results and idealized analytical models show good agreement between design assumptions and actual properties of the pendulum rocking wall system.

Keywords: Cross-laminated timber, seismic resiliency, rocking walls, rolling inverted pendulum, slip-friction inverted pendulum

Introduction

Cross-Laminated Timber (CLT) panels, since originating in Europe over two decades ago, have revolutionized the design of modern heavy timber structures worldwide (Pei et al. 2016). CLT production assembles large volumes of lumber, in at least three orthogonal layers, for pressing and adhesion into structural composite panels that work as slab, deck, or wall systems (ANSI/APA PRG 320 2018). As a composite panel resembling precast concrete in size, CLT delivers economic, environmental, and structural performance benefits leading to more effective use of wood, smaller carbon footprints, and weight savings in commercial construction. Nearly a decade ago, Murray Grove, a 9-story apartment building in London, drew international focus on CLT construction with its fully panelized platform structure rising several stories taller than conventional timber framing (TRADA 2009). Shake-table tests of a 7-story CLT platform assembly, however, called seismic performance into question, after registering peak acceleration of 3.8 g in the upper floor (Ceccotti et al. 2013). Early renditions of CLT platform construction, therefore, need new design approaches before entering earthquake hazardous regions.

CLT construction promises multifaceted revitalization for the western United States—where sizable forest products economies, sustainable building markets, and seismic hazards coincide. Despite inherent lightweight capability to reduce seismic excitation mass, few CLT buildings have been constructed in earthquake regions, because

continued on next page

alternatives to codified structural schemes carry an extra burden of proof (ASCE/SEI 7 2017). Design of the 12-story Framework building earned permitting in Portland, Oregon, for its vertically post-tensioned CLT rocking wall lateral system and flexible mass timber frame, via validation testing and peer review, yet the project remains unrealized for lack of financing (Zimmerman and McDonnell 2017, Zimmerman and McDonnell 2018). In contrast, the 18-story Brock Commons, built with a predominantly mass timber structure in Vancouver, British Columbia, expedited approval of the lateral force-resisting system by pairing the timber gravity system with prequalified reinforced concrete cores (Fast and Jackson 2017). Though currently less expedient, treating CLT as an emerging technology with its own advantages is leading to better lateral systems.

To expand the effectiveness of CLT lateral systems, the "Structural Research Drive" maps seismic development with *code minimum*, *code plus*, and *resilient* hierarchical tiers of performance expectations (Pei et al. 2014, Pei et al. 2016). Determining seismic design parameters for CLT, via rigorous FEMA P695 qualification procedures, fulfills essential code requirements that lay a foundational tier of objectives (Applied Building Technology Council 2009, Amini et al. 2014). CLT systems, however, must target the pinnacle of seismic performance with *resilient* solutions to extend the most compelling approach (Pei et al. 2014, Pei et al. 2016). Recent tests of vertically post-tensioned rocking CLT walls, adapted from pioneering research in precast concrete, offer ways to achieve resilience (Dunbar et al. 2014, Ganey et al. 2017). Shake-table tests of a 2-story timber structure of vertically post-tensioned walls, diaphragms, and glulam framing, produced no significant damage, further demonstrating resilience with an entire assembly(Pei, van de Lindt, et al. 2018). Future shake-table tests will soon examine 10-story timber archetypes featuring various vertically post-tensioned CLT walls (Pei, Berman, et al. 2018).

For vertically post-tensioned rocking wall systems to work effectively, unbonded tendons must bear on top of walls and anchor into foundations to safeguard walls from overturning. Post-tensioned walls generally span full building height to best support all diaphragms laterally. CLT panels usually extend past several floors to minimize horizontal wall joints, and connections between wall panels and intersecting floors must enable rocking without constraint. Rocking walls, moreover, must be slenderly proportioned to take advantage of the counterintuitive "scale effect" of rectangular inverted pendulum blocks, first elucidated by Housner (1963, p. 417). Pivoting on the base corners of rectangular walls, in fact, drives the rocking mechanism and opens gaps that engage vertical tendon restraints. Vertically post-tensioned rocking walls, therefore, typically entail *rectangular* panels and *balloon* construction.

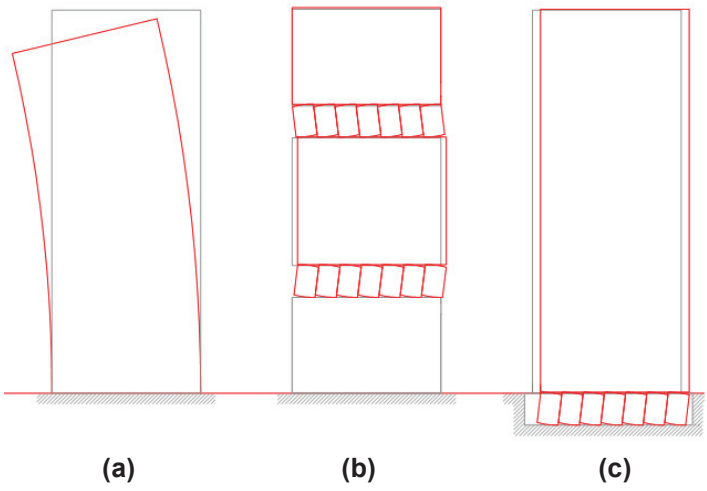

Figure 1: Elevations views of (a) Fixed base, (b) multiple soft-story rocking, and (c) soft-story rocking base schemes.

An alternative *elliptically profiled* rocking wall panel can integrate with *platform* construction to self-center without post-tensioning. Platform assembly, in contrast to balloon, simplifies construction sequencing and connection details with one-story tall modular components. Figure 1 illustrates three building schemes, in elevation views, for

continued on next page

comparison. View (a) cantilevers from the ground and funnels forces to the base, representing how most commonly designed buildings behave under lateral effects. Views (b) and (c) introduce soft-stories designed to flex laterally and self-center under superstructure weight. Soft stories can divide superstructures into multiple blocks, as shown in view (b), or support the entire superstructure above grade level, as shown in view (c). Because soft stories undergo virtually all lateral inter-story drift, superstructure blocks can comprise of any rigid construction that CLT walls can support at the rocking level. The following sections of this article detail mechanics and performance of a one-story tall elliptical rocking wall prototyped in CLT, with focus on timber contact boundaries critical to the pendulum system.

Shaping an Elliptical Rolling Pendulum Made of Timber

Figure 2 illustrates the concept of the passive self-centering platform CLT wall proposed here. Early research of construction assemblies demonstrated that various boundary conditions alter the rocking response of rectangular CLT shearwall panels (Dujic and Zarnic 2006). While rectangular panels may rock in a platform assembly, the rotated panel of Figure 2 shows corners protruding into ceiling and floor space. Curving load-bearing edges whittles the corners to facilitate panel rotation. Study of circular, elliptical, and parabolic half disks has demonstrated that geometric properties, such as radius or proportions of width and height, control various characteristics of inverted pendulum rocking (Mazzoleni et al. 2015). Within a platform assembly, ellipse eccentricity uniquely leverages superstructure weight to provide restoring moment. This project prototypes elliptical geometry to take advantage of distinctive passively self-centering features.

Elliptical Rolling Pendulum Mechanics

Figure 3 illustrates a panel that fits the middle of an elliptical profile to adapt ellipse geometry to wall construction. The mathematical model, forming the basis of Figure 3, was initially developed to analyze elliptical rolling rods as seismic isolation (Jangid and Londhe 1998, Londhe and Jangid 1999). The

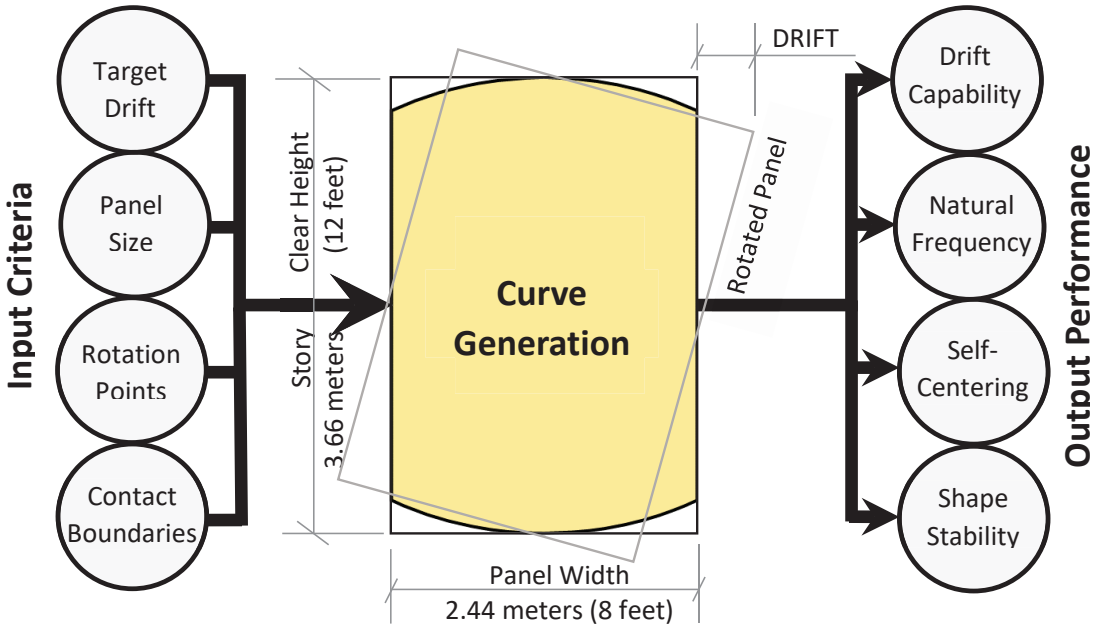

Figure 2: Shaping CLT Panels for Rocking Response to Earthquakes

continued on next page

original application placed a multistory structural frame atop elliptical rolling rods of varying eccentricity, e, quantified by:

$$e = \sqrt{1 - \frac{b^2}{a^2}}$$

where $\boldsymbol{a}$ = semi-major axis length and $\boldsymbol{b}$ = semi-minor axis length of the parent ellipse. Cross-sections of the rolling rods formed complete ellipses, but mechanics of the rolling pendulum still apply to the truncated panels shown in Figure 3.

Two fundamental assumptions establish the rocking wall response diagrammed in Figure 3. First, the floor and ceiling that sandwich the rocking wall should remain horizontal, as rigid bodies throughout the rolling response. Structural design practice commonly fulfills this rigid-body condition with beams and superstructures conforming to standard serviceability criteria. Following rigid-body constraint, view (a) assigns 3 independent degrees of freedom to the panel, x_r, y_r, and θ_r, and only 2 translational degrees of freedom, x_b and y_b, to the dependent supported mass.

Secondly, elliptical arc length, AA'' or BB'', equals the respective straight horizontal segment of ceiling, AA', or floor, BB', between contact points shown in Figure 3 view (b). Relative slip between the rocking wall and the bounding floor and ceiling should be either eliminated or neutralized. Slippage, if unconstrained, threatens to introduce residual displacements that negate the self-centering benefits of the pendulum system. Because friction between the rocking wall and bounding floor and ceiling presents uncertainty, traction cannot completely enforce non-slip kinematic conditions. To ensure that walls roll without slipping, *displacement restraints* connect the panel to the floor and

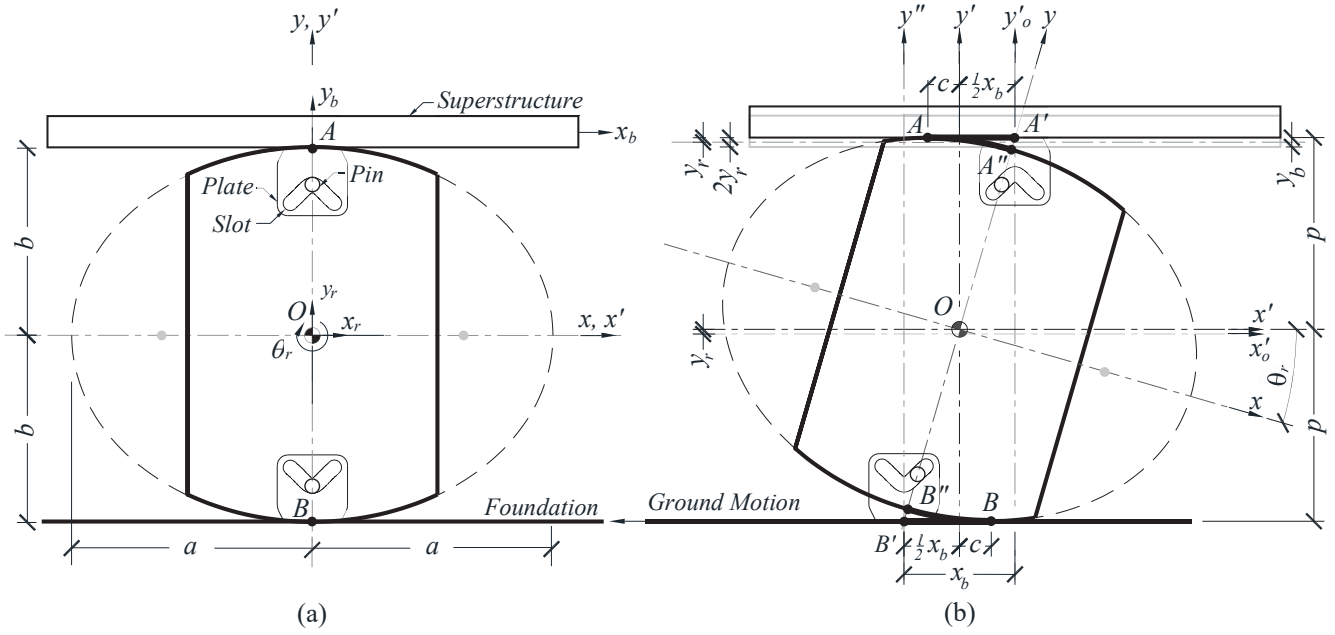

Figure 3: Rolling Elliptical Pendulum Model, Adapted to Load-Bearing Wall Panel from (Jangid and Londhe)

continued on next page

ceiling with pins and slotted plates as depicted in Figure 3. Faceplates connected to ceiling and floor beams guide panels to roll in plane, with slots that direct pin travel. If slip occurs in the Figure 3 configuration, pins bear against all components, panel and faceplates, but with minimal connection constraint. A similar shear key connection concept approximated paths of pin travel for a rectangular rocking timber panel and calculated effects of connection constraint (Loo et al. 2014). The v-shaped slots pictured in Figure 3 take shape by tracing connection points of the rolling ellipse through a desired range of lateral displacements, to minimize constraint.

Figure 4 diagrams main forces on the free-body of a rolling panel configured, according to Figure 3, to transfer shear primarily via traction at load-bearing edges. Summation of moments about point *O* for equilibrium arrives at the lateral force estimation, F_L, offered by Jangid and Londhe:

$$F_L = W\left(\mu_r \, sgn(\dot{x_b}) + \frac{c}{p}\right)$$

where W is the superstructure weight transferred through the directly supported mass; μ_r is a rolling friction coefficient; the *signum function* specifies the direction of horizontal traction forces, and dimensions c and p respectively indicate half the moment arm distance of the vertical restoring moment and horizontal overturning moment induced by traction. Neglecting panel weight typically results in conservative design or no appreciable effect, because panel weight, w_p, typically adds to the restoring moment and amounts to minute fractions of the total supported weight.

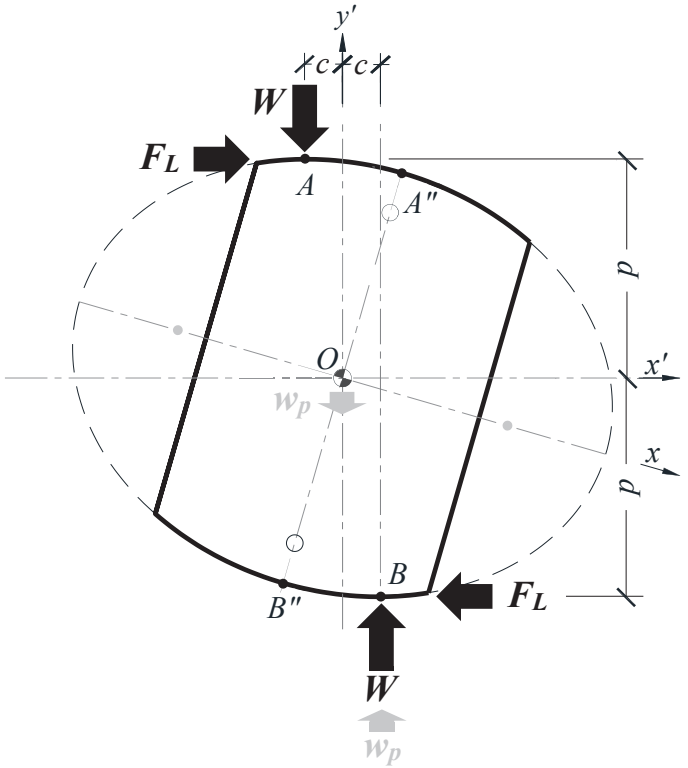

Figure 4: Free-Body Diagram of Edge Contact
(rolling friction and inertial forces not shown for clarity)

continued on next page

Figure 5 plots an idealized hysteresis loop that normalizes superstructure weight, W, with lateral force F_L, expressed as a function of the lateral drift ratio, $x_b/2b$:

$$F_L\left(\frac{x_b}{2b}\right) = W\left(\mu_r\, sgn(\dot{x}_b) + \frac{c}{p}\cdot\frac{x_b}{2b}\right).$$

Rolling friction coefficient, μ_r, determines the y-intercepts of the normalized lateral force function and depth of the hysteresis loop. Because rolling friction dissipates little energy, Figure 5 charts a narrow hysteresis loop estimating the magnitude of rolling friction at 1% of overburden weight. The c/p ratio of dimensions, labeled in Figures 3 and 4, charts stiffness that behaves nonlinearly but only slightly so within the practical range plotted by the solid lines. A circle, or ellipse of zero eccentricity, acts as a roller providing virtually no lateral stiffness. An ellipse of maximum eccentricity, approaching unity, essentially matches the stiffness of a rectangular panel. Figure 5 presents an ellipse of eccentricity, e, equal to 0.73, to demonstrate properties of a prototype panel with high lateral drift capacity and low stiffness, relative to a conventionally anchored shearwall.

Elliptical Slip-Friction Pendulum Mechanics

Figure 6 illustrates a vertically slotted connection plate that transfers story shear primarily through horizontal pin constraints, instead of relying on traction. Horizontal constraint forces the panel to rotate about the pins and contact surfaces to slip along distances, x_c, dimensioned in Figure 6. Lateral displacement of the newly constrained configuration, x_p, relates to the previous rolling mechanism via equation: $x_p = x_b - 2x_c$. Though the net lateral displacement of x_p is less than x_b, for a given panel rotation θ_r, the path effectively traveled by the constrained system measures $2x_c$ greater than x_b.

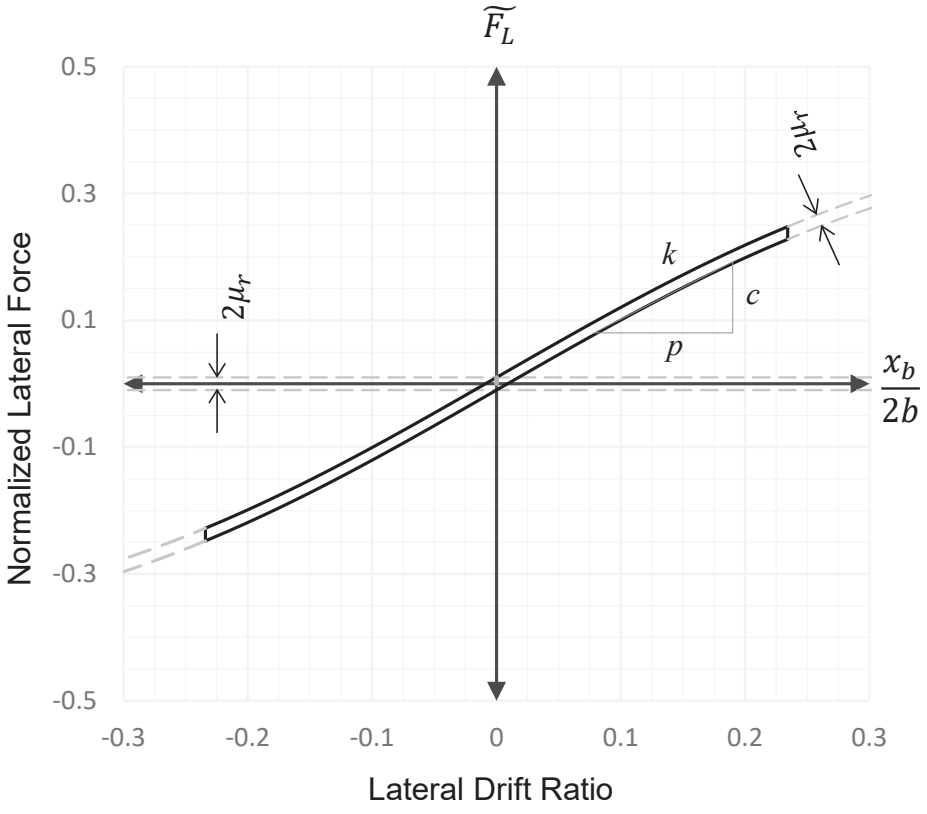

Figure 5: Normalized Lateral Stiffness Plot for No-Slip Rolling Elliptical Panels of Eccentricity, *e = 0.73*

continued on next page

Proportioning similar triangles expresses the cumulative path of travel as:

$$x_b + 2x_c = \left(\frac{2p}{d\cos\theta_r} - 1\right)x_p.$$

Pushing panels with greater force through the same rotation, θ_r, but with less translation, increases effective lateral stiffness. Sliding, furthermore, creates frictional forces, F_S, as shown in Figure 7. In addition to friction between timber and steel, steel-to-steel contact between pins and face plates generates sliding friction, f_p, and pins spinning within pipe bushings embedded in the timber panel generate rotational friction. Globally, the model does not consider the force couple produced by f_p as restorative but aggregates sources of frictional damping into a sum of rolling and sliding, μ_r and μ_s, coefficients. Pins counteract sliding forces and transfer story shears on a moment arm reduced from $2p$ between edge contact points to $2d\cos\theta_r$ between pin centers. Considering the effective travel and moment arm between pin centers, yields pin force, F_p, expressed as a function of net lateral displacement, x_p:

$$F_P(x_p) = W\left((\mu_r + \mu_s)\ sgn(\dot{x_p}) + \frac{c}{d\cos\theta_r}\left(\frac{2p}{d\cos\theta_r} - 1\right)x_p\right).$$

Figure 8 normalizes lateral force, F_p, and plots the relationship with respect to lateral drift ratio, $x_p/2b$. Comparisons of Figure 8 with the no-slip traction of Figure 5 reveal significant differences. Sliding friction increases the y-intercept of Figure 8 so that the sum of frictional coefficients totals 10% raising the rocking threshold and adding hysteretic damping. Connection constraint, furthermore, significantly reduces the range of lateral displacements. Within a practical range, the slip-friction system behaves nearly linearly, but the dashed trends of Figure 8 indicate a stiffening effect. Pin contact with vertical limits of the slots should, by design, stiffen and restrain the system from venturing beyond the practical, solid-line regions of the mathematical functions.

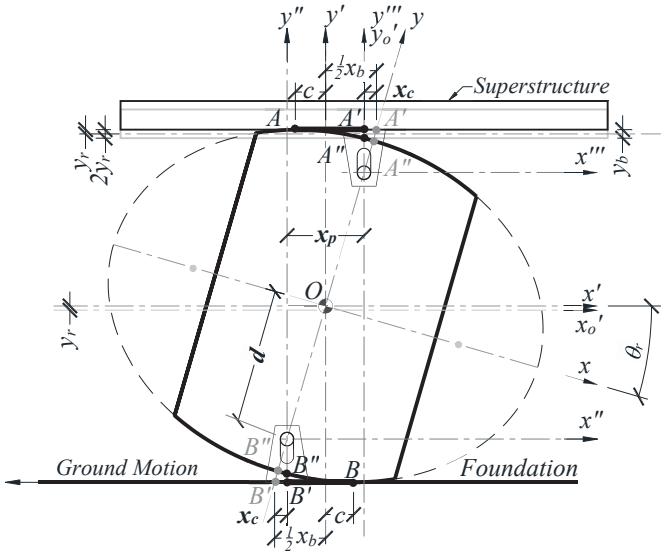

Figure 6: Slip-Friction Pendulum Model

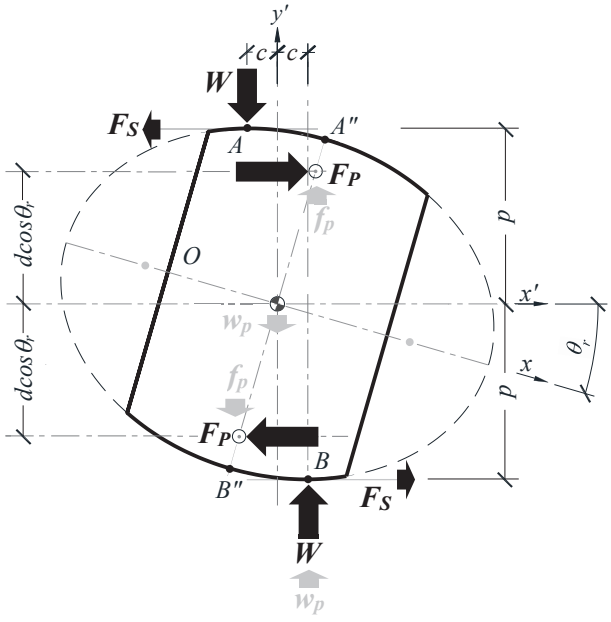

Figure 7: Free-Body Diagram Including Pin Contact
(rolling friction of the panel, rotational friction of the pins, and inertial forces not shown for clarity)

continued on next page

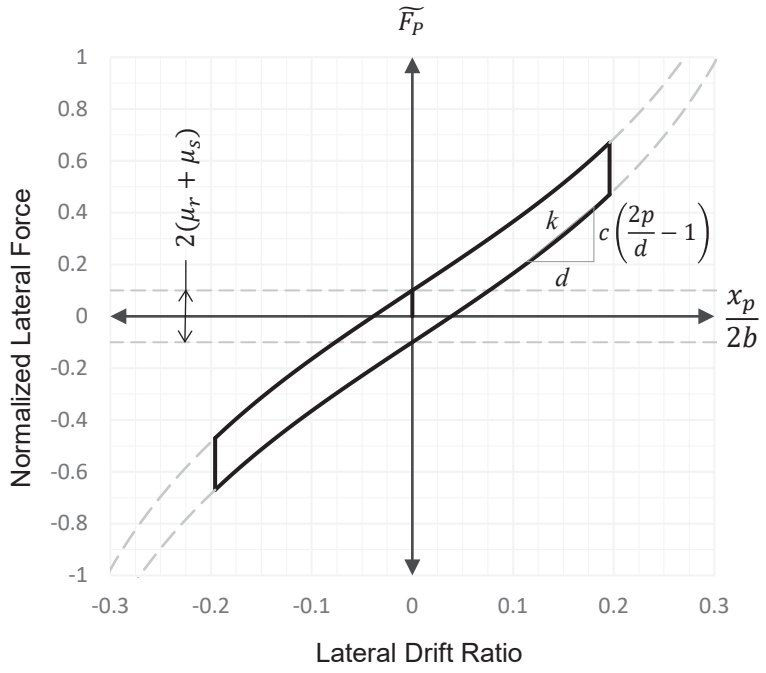

Figure 8: Normalized Lateral Stiffness for Slip-Friction Rolling Elliptical Panels of Eccentricity, *e = 0.73*

Prototype Performance

The *No-Slip Traction* and *Slip-Friction* rocking models hypothesize that:

- Rigid-body mechanics can estimate lateral stiffness properties of full-scale CLT panels with reasonable accuracy,
- Slot shape of the faceplate connections determines the rocking mode, by varying connection constraint, and
- CLT can endure concentrated, high-pressure compression bearing contact and shear induced by friction, with only localized damage while maintaining overall structural stiffness.

Prototype Testing

Figure 9 renders laboratory test apparatus around a full-scale, 5-ply CLT prototype—measuring 2.44 m by 3.66 m by 0.170 m (8 ft by 12 ft by 6.625 in.) in respective width, height, and thickness—and conforming to North American manufacturing standards for grade V2M1 (ANSI/APA PRG 320 2018). CNC fabrication cut the CLT panel to an elliptical profile of semi-major axis width, *a*, and semi-minor axis height, *b*, respectively equaling 2667 mm (105 in.) and 1829 mm (72 in.). CNC also bored holes through the CLT at pin locations specified by digital drawings and similarly processed steel to plasma-cut the slotted connections diagramed in

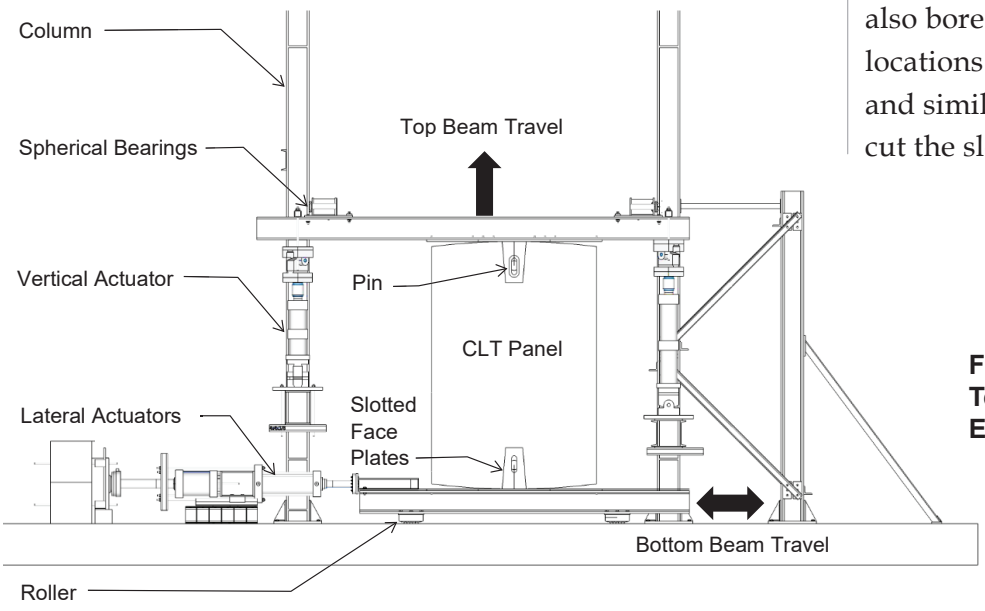

Figure 9: Full-Scale Prototype Test Specimen and Apparatus Elevation View

continued on next page

Figures 3 and 6. A steel support structure framed CLT specimens with fixed and moving parts to create boundary conditions of a rocking soft story. Horizontally oriented actuators applied lateral force to the bottom beam, which glided on industrial rollers within a channel track. Vertically oriented actuators simulated superstructure weight through a feedback process that kept the top beam level and maintained a constant sum of load, while simultaneously adjusting to the moving panel contact point. Accommodating rocking yet preventing overturning, the top assembly of 3 steel beams traveled strictly vertically, gliding on spherical bearings rolling on plates fixed to the column flanges. Precautionary out-of-plane bracing typically did not engage, because wall panels rolled within tolerances set by gaps between braces and panel faces.

Table 1: Cyclic Prototype Test Protocol, adapted from Chapter 17 of *ASCE/SEI 7-16*

Displacement Step	Number of Cycles
$0.0025h_s$	20
$0.25D_M$	3
$0.50D_M$	3
$0.67D_M$	3
$1.00D_M$	6
$0.75D_M$	$\frac{30S_{M1}}{S_{MS}B_M} = \mathbf{18} \geq 10$

h_s = story clear height = 3.66 m (12 ft)

D_M = in-plane maximum lateral displacement, limited by panel geometry or external connection limits.

S_{M1} = the MCE_R, 5% damped, spectral response acceleration parameter at a period of 1s adjusted for site class effects

S_{MS} = the MCE_R, 5% damped, spectral response acceleration parameter at short periods adjusted for site class effects

B_M = Numerical coefficient depending on effective damping, β_M, percentage of critical.

Because rocking walls undergo displacement excursions much larger than the the lateral displacement capacities of conventional shearwalls, test protocols emulated quasi-static prototyping procedures for seismic isolation (ASCE/SEI 7 2017). The test protocol of Table 1 generally follows code for seismic isolation but requires simplifying assumptions for first-iteration prototypes. Cycles at the first displacement step represent wind drift limits. Subsequent displacement steps and cycles assess seismic demands.

The same CLT panel specimen was subjected to the Table 1 displacement protocol under two different configurations:

1. *No-Slip Traction Rolling* under simulated superstructure gravity load, or overburden, of 400 kN (90 kips), and
2. *Slip-Friction Rocking* under a low overburden of 133 kN (30 kips).

Synchronized load cells and displacement transducers of the hydraulic actuator system supplied the primary data used to assess properties of the rocking wall system.

Hysteretic Performance

Table 2 summarizes key results of the two test configurations. Figures 10 and 11 respectively plot lateral load versus lateral displacement for *No-Slip Traction Rolling* and *Slip-Friction Rocking* of a one-story tall, 5-layer CLT panel at each seismic displacement milestone of the Table 1 cyclic protocol. In the *No-Slip Traction Rolling* case, two horizontal actuators stroked in series to provide fully reversed cycles approaching ± 432 mm (± 17 in.) and unidirectional cycles up to 864 mm (34 in.), utilizing full lateral displacement capacity of the apparatus. Geometric relationships of the rolling elliptical pendulum, corresponding to Figures 3 through 5, independently shaped the idealized hysteresis superposed on plots of the Figure 10 test data. Estimating the depth of the idealized hysteresis, however, required readings at the onset of lateral displacement to calibrate frictional effects.

continued on next page

Table 2: Summary of Lateral Stiffness Derived from Cyclic Tests of 5-Layer CLT Panel with e = 0.73

Connection Configuration	Overburden W		Hysteretic Friction Coeff. μ	Stiffness*				Maximum Tested Lateral Displacement D_M	
				Measured		Normalized to unit of overburden force			
	(kN)	(kips)	(% of W)	(kN/mm)	(kips/in.)	x 10^{-4} (kN/mm)	x 10^{-3} (kips/in.)	(mm)	(in.)
No-Slip Traction	400	90	1	0.120	0.68	3.00	7.56	864	34.0
Slip-friction	133	30	10	0.095	0.54	7.14	18.00	717	28.2

*Values derived from test data using secant tangent stiffness at $0.5D_M$

A rolling friction coefficient of μ_r equal to 1% of the overburden weight estimated frictional damping reasonably well through displacements up to half of the maximum tested limit.

Figure 10 plots (a) and (b) indicate close agreement between theoretical model and experimental results. Slope of actual hysteresis loops over the range of fully reversed cycles matched the mathematical stiffness model, and uniform spacing between top and bottom segments of the hysteresis exhibited constant damping. Recessed steel floor anchorages, not quite flush with the concrete surface, and continuous track mechanisms of industrial rollers supporting the bottom beam contributed minor and regular blips to the recorded data, noise attributable to imperfections of the setup rather than the prototype.

Beginning with the $0.67D_M$ step in Figure 10 plot (c), however, unidirectional cycles inflated hysteresis loops. Local splitting of timber in bearing contact zones, steel yielding along slots of pin bearing, and friction of moving test apparatus all likely added damping that the idealized model did not track. Beyond lateral displacement of $0.75D_M$, the idealized hysteresis model, furthermore, did not account for an observed stiffness increase. Contact of panel corners could have caused the apparent stiffness to increase near extreme lateral drift. Throughout the entire tested range, actual hysteresis loops essentially retraced paths, indicating no appreciable damage.

Figure 11 plots the hysteretic performance of the same panel, subsequently configured according to the slip-friction model presented in Figures 6 through 8. The specimen, prior to testing in slip-friction, had experienced the load history of traction rolling charted by Figure 10, which preconditioned the load-bearing edges, but without significant damage to the CLT panel. Peak lateral force, F_P, registered at maximum lateral displacement D_M increased by 8% in comparison with the maximum F_L of Figure 10, while D_M decreased by 17% because of added horizontal connection constraint. Despite higher peak lateral force, the panel configuration of Figure 11 supported only a third of the overburden, 133 kN (30 kips), relative to the previous setup. Sliding added frictional damping forces amounting to 9% of the overburden. The idealized hysteresis of Figure 11, therefore, cumulatively considered rolling and sliding friction with a summation of coefficients:

$$\mu = \mu_r + \mu_s = 0.01 + 0.09 = 0.10$$

to model total frictional damping and set the depth of the idealized hysteresis loop.

continued on next page

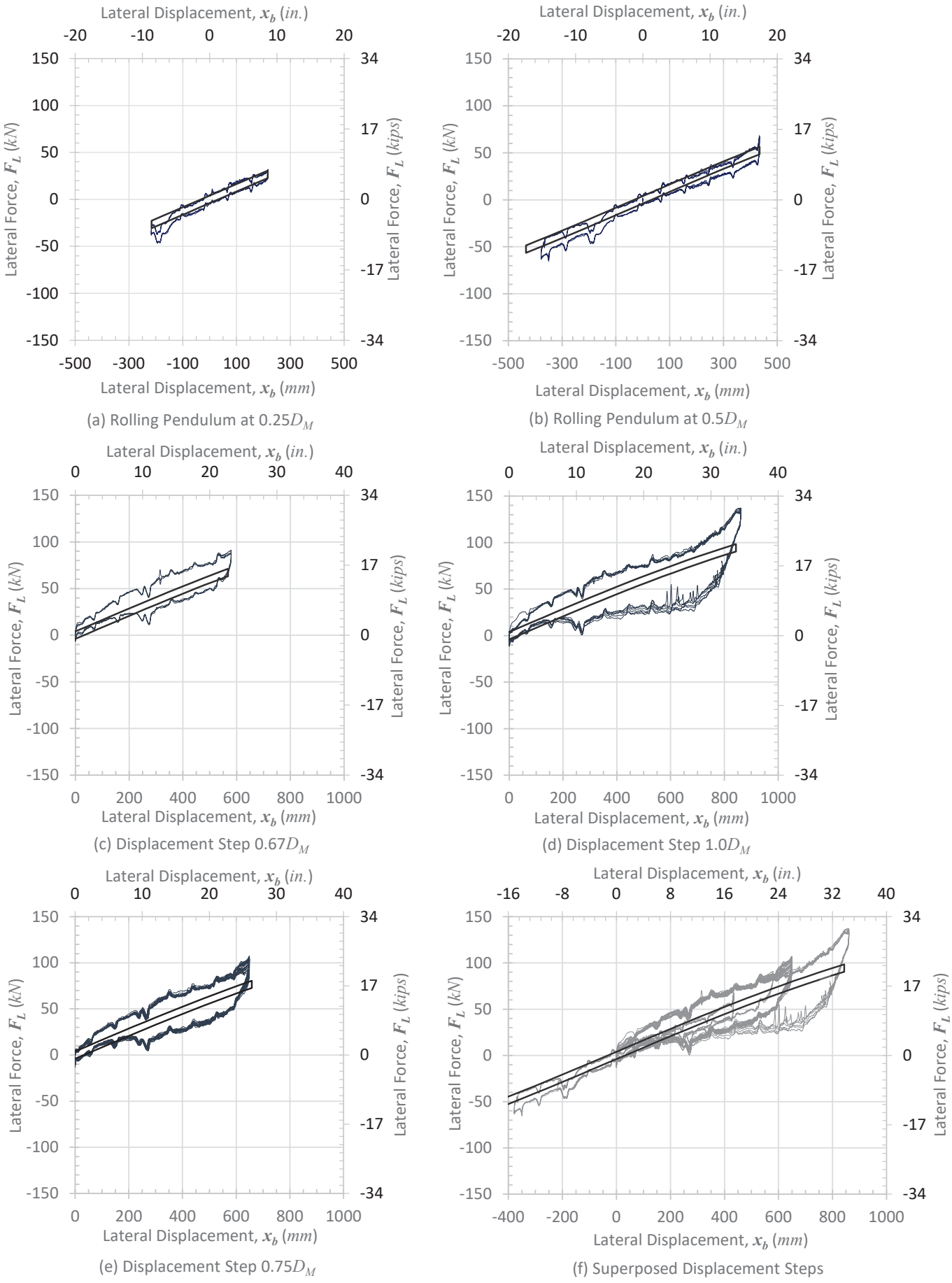

Figure 10: Hysteresis Plots of No-Slip Traction Configuration of e = 0.73 Panel under High Overburden of 400 kN (90 kips)

continued on next page

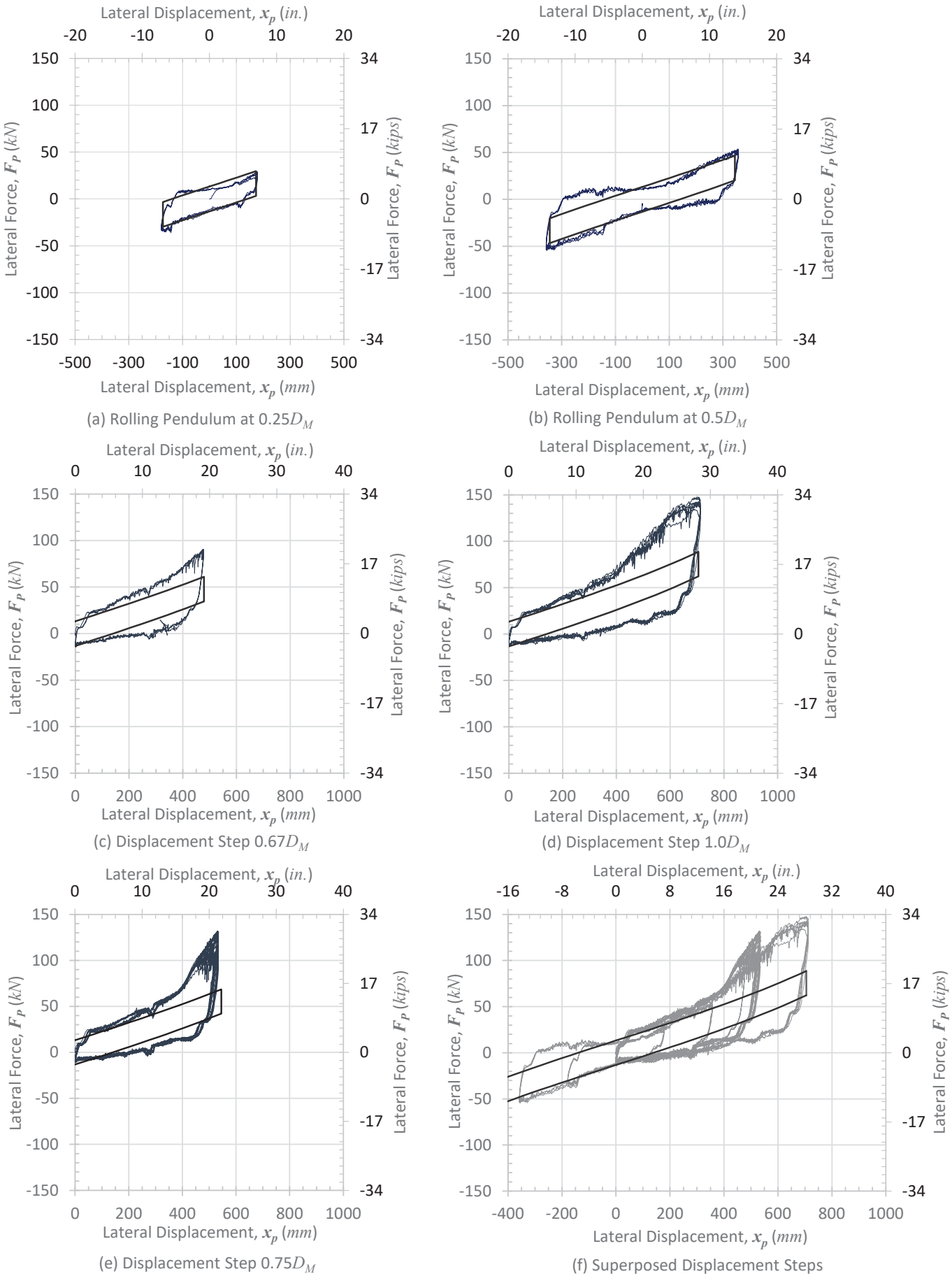

Figure 11: Hysteresis Plots of Slip-Friction Configuration of e = 0.73 Panel under Low Overburden of 133 kN (30 kips)

continued on next page

Theoretical and empirically measured hysteresis loops indicate reasonable agreement through the ± 356 mm (± 14 in.) range of fully reversed cycles. Plot (a) shows the top right loading branch of the empirical hysteresis dipping below the theoretical model, but the remaining segments behaved predictably. Plot (b) shows a similar dip, but the loading branch of the lower left quadrant charted as expected. Stiffness of the panel in plots (a) and (b) matched slopes of the idealized hysteresis loop through the reversed cycles. Plots of the unidirectional half cycles, however, show that stiffness of the slip-friction system rose more rapidly at outer reaches of lateral displacement than the gradual increase predicted by mathematical modeling.

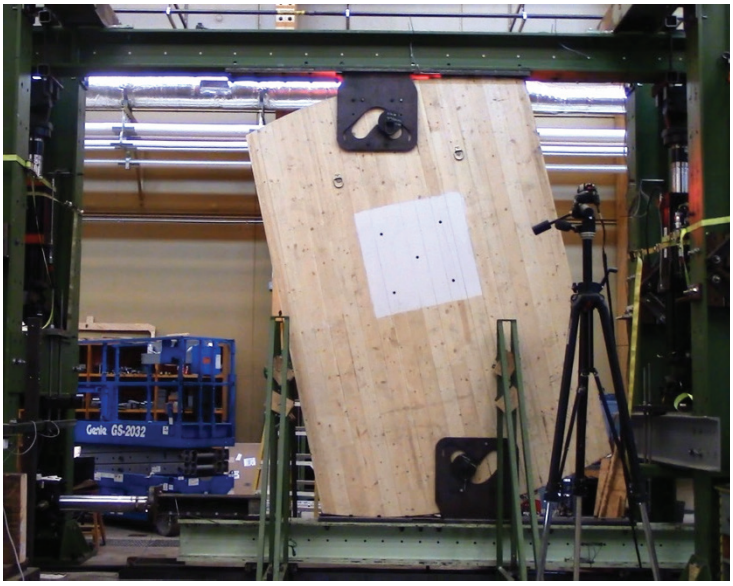

Figure 12: Rolling of e = 0.73 Panel at Max Lateral Displacement and Overburden of 400 kN (90 kips)

Observed Damage

Figure 12 photographed the test specimen charted in Figure 10 (d) near extreme lateral displacement at approximately 13º of panel rotation. Figure 13 exhibits staining of the bottom panel edge photographed immediately following unidirectional cyclic tests in the *No-Slip Traction Rolling* configuration. Staining on the left half indicated travel of the contact point. Fully reversed cycles of previous tests left barely discernable signs of contact on the right half. Figure 14 provides a closeup view of the local crushing of timber end grain observed in the longitudinal CLT laminations at the outer reach of the contact. Laminations split when the component of contact bearing force oriented perpendicular to grain exceeded tension strength of the timber. Both traction forces and eccentricity of the wood grain, with respect to gravity loads, grew as the panel rotated. Longitudinal laminations bore the brunt of the damage, because virtually all axial compression in the CLT panel transfers parallel to grain. Cross-laminations, however, restrain splits in the longitudinal laminations.

Figure 13: Bottom Edge of e = 0.73 Panel after Unidirectional Rolling Tests

Figure 14: Local Damage of Bottom Edge of e = 0.73 Panel after Unidirectional Rolling Tests

continued on next page

Figure 15 photographed the same specimen and panel rotation but in *Slip-Friction Rocking* configuration corresponding to plot (d) of Figure 11. Figure 16 enlarged the view of the top right corner to show where gaps between and splits within laminations opened and closed because of sliding. Video captured movements of laminations as the contact point traveled along the top edge and accompanying audible pops. Sliding produced noticeably louder creaking than the crackles recorded during rolling configuration tests. Figure 17 photographed splits and scrapes of the top panel edge immediately following the unidirectional tests charted by Figure 11. Sliding exacerbated splits in the longitudinal laminations and at only a third of the overburden load that caused lesser damage in rolling. Figure 11 plots (c) through (f) captured some effects of the stick-slip frictional behavior in noise of loading segments. Stick-slip friction posed little consequence to overall stiffness of the CLT panel but caused noticeably higher damage to panel edges. Reverberating booms, furthermore, dynamically impacted and eventually dislodged pipe bushings embedded in the CLT in later tests at higher overburden.

The local damage observed in both rolling and slip-friction configurations could be mitigated by adding cross-laminations to the faces of the 5-ply panel. Outer cross layers may serve as both protective cover for the longitudinal plies and transverse reinforcement counteracting cracks induced by traction or sliding. Though the panel from the *No-Slip Traction Rolling* test was reused for slip-friction rocking tests, a new panel tested in *Slip-Friction Rocking* would likely sustain similar damage. Design modifications therefore should address concentrations of force in the timber near the pinned connections.

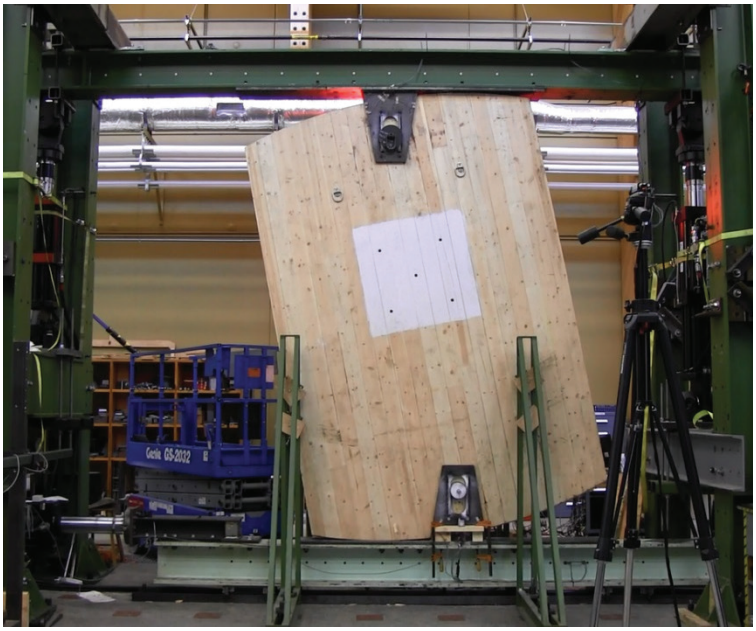

Figure 15: Slip-Friction of e = 0.73 Panel at Max Lateral Displacement and Overburden of 133 kN (30 kips)

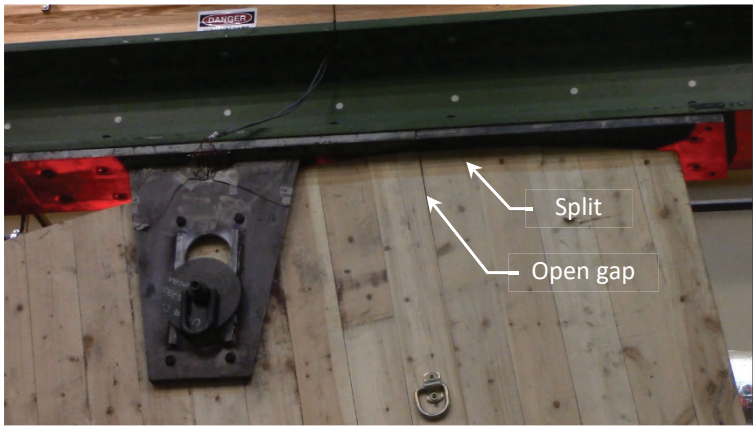

Figure 16: Splits and Gaps Open during Slip-Friction Sliding at Top Contact Bearing Zone.

Figure 17: Local Damage of Top Edge of Panel after Unidirectional Slip-Friction Tests

continued on next page

Conclusions

- As a rigid body, the CLT prototype panel generally behaved predictably, according to principles of mechanics.
- Elliptical eccentricity provided the key feature for passive self-centering within a platform construction scheme.
- Connection constraints dictated the modes of horizontal shear transfer and rocking.
- Curvilinear pin slots shaped to act only as *displacement restraints* imposed minimal constraint, which enabled the elliptical panel to rock as a *rolling pendulum*.
- Vertical slots imposed horizontal connection constraint, which forced the panel into a *slip-friction* mechanism.
- Idealized hysteresis models enveloped the observed behaviors of the physical prototype with reasonable accuracy through lateral displacements ranging between:
  - ◊ ±432 mm (17.0 in.) in *No-Slip Traction Rolling*, and
  - ◊ ±356 mm (14.0 in.) in *Slip-Friction Rocking*.
- Idealized rigid-body models underestimated both damping and stiffness at extreme lateral displacements.
  - ◊ Simplifications in the *slip-friction rocking* model,which assume an aggregate and constant sliding friction force throughout the motion, do not keep pace with the rapid stiffness and damping increases observed at larger lateral displacements.
- *No-Slip Traction Rolling*, compared to *Slip-Friction Rocking*, demonstrated:
  - ◊ More than 3 times greater capacity for carrying superstructure weight on the same panel specimen, before damage to critical timber laminations begins.
  - ◊ 17% greater lateral displacement capacity for the same panel rotation limit, and
  - ◊ 2 times lesser lateral stiffness for the same overburden.
- Rolling produced less damage than sliding at the timber contact zones along panel edges.

Key takeaways from this first iteration of analytical and physical prototyping suggest that *rolling* is more resilient than the *slip-friction* pendulum. Frictional energy dissipation increased wear of CLT panel, lateral stiffness of the system, and concentrated forces at pin connections. Resilience of the *slip-friction* configuration, however, can likely improve with simple strategies. Adding cross-plies to the outer wall faces, for example, would confine and reinforce the axial-load-carrying laminations. Shoes fit to the edges of the CLT panel could alternatively produce smoother sliding and distribute bearing contact forces over a greater area of timber. Refining details of the slip-friction panel mechanism, furthermore, would enhance versatility of the elliptical inverted pendulum concept. While the *rolling* configuration provides better seismic isolation properties in the direction of the wall plane, the slip-friction configuration offers several benefits other than better energy dissipation, such as:

- Universal connections that are interchangeable with a variety of elliptical profiles,
- Reduced risk of residual lateral displacements, and
- Higher thresholds to rocking, which improves everyday resistance to wind.

To better characterize the *slip-friction rocking* mechanism, an analytical model based on mechanical work equations is being developed. Multiple sources of friction, including frictional bearing contact of the pin connections, likely contribute to the nonlinear effects most pronounced by the hysteresis data at extreme lateral displacements. In conclusion, both *rolling* and *slip-friction* pendulum configurations merit further refinements because each showed

continued on next page

potential to improve the resiliency, versatility, and economic competitiveness of mass timber platform construction in regions of high seismicity.

Acknowledgement

The U.S. Forest Service in cooperation with the University of Wisconsin-Milwaukee funded this research through the Wood Innovations Program (Grant Number: 2016-DG-11420004-170). The U.S.D.A. Forest Products Laboratory–Engineering Mechanics and Remote Sensing Laboratory (Madison, Wisconsin) performed full-scale testing. The findings and opinions of this article represent views of the authors, which do not necessarily represent those of the sponsors.

References

Amini, M.O., J.W. van de Lindt, S. Pei, D.R. Rammer, P. Line and M. Popovski (2014). Overview of a project to quantify seismic performance factors for cross laminated timber structures in the United States. In: Materials and joints in timber structures. S. Aicher, H.-W. Reinhardt and H. Garrecht, Springer, Stuttgart, Germany**:** 531-541.

ANSI/APA PRG 320 (2018). Standard for Performance-Rated Cross-Laminated Timber. Tacoma, Washington, APA—The Engineered Wood Association**:** 1-40.

Applied Building Technology Council (2009). Quantification of Building Seismic Performance Factors, FEMA P695. Washington D.C., Federal Emergency Management Agency (FEMA).

ASCE/SEI 7 (2017). Chapter 12: Seismic Design Requirements for Building Structures. In: Minimum Design Loads and Associated Criteria for Buildings and Other Structures (ASCE/SEI 7-16), American Society of Civil Engineers, Reston, VA, USA**:** 89 - 119.

ASCE/SEI 7 (2017). Chapter 17: Seismic Design Requirements for Seismically Isolated Structures. In: Minimum Design Loads for Buildings and Other Structures (ASCE/SEI 7-16), American Society of Civil Engineers, Reston, VA, USA**:** 168-179.

Ceccotti, A., C. Sandhaas, M. Okabe, M. Yasumura, C. Minowa and N. Kawai (2013). SOFIE project – 3D shaking table test on a seven-storey full-scale cross-laminated timber building. In: Earthquake Engineering & Structural Dynamics. 42**:** 2003-2021.

Dujic, B. and R. Zarnic (2006). Study of lateral resistance of massive X-lam wooden wall system subjected to horizontal loads. International Workshop on Earthquake Engineering on Timber Structures. Coimbra, Portugal, COST E29- European Cooperation in the Field of Scientific and Technical Research**:** 97-104.

Dunbar, A.J.M., S. Pampanin and A.H. Buchanan (2014). Seismic performance of core-walls for multi-storey timber buildings.

Fast, P. and R. Jackson (2017). Brock Commons: A Case Study In Tall Timber. STRUCTURE magazine. Reedsburg, Wisconsin, C3 Ink. 24**:** 50 - 52.

Ganey, R., J. Berman, T. Akbas, S. Loftus, J. Daniel Dolan, R. Sause, J. Ricles, S. Pei, J.W. van de Lindt and H.-E. Blomgren (2017). Experimental Investigation of Self-Centering Cross-Laminated Timber Walls. In: Journal of Structural Engineering. 143.

Housner, G.W. (1963). The behavior of inverted pendulum structures during earthquakes. In: Bulletin of the seismological society of America. 53**:** 403-417.

Jangid, R.S. and Y.B. Londhe (1998). Effectiveness of Elliptical Rolling Rods for Base Isolation. In: Journal of Structural Engineering. 124**:** 469-472.

continued on next page

Londhe, Y.B. and R.S. Jangid (1999). Dynamic response of structures supported on elliptical rolling rods. In: Doboku Gakkai Ronbunshu. 612**:** 11-20.

Loo, W.Y., C. Kun, P. Quenneville and N. Chouw (2014). Experimental testing of a rocking timber shear wall with slip-friction connectors. In: Earthquake Engineering & Structural Dynamics. 43**:** 1621-1639.

Mazzoleni, M.J., M.B. Krone and B.P. Mann (2015). Dynamics of Rocking Semicircular, Parabolic, and Semi-Elliptical Disks: Equilibria, Stability, and Natural Frequencies. In: Journal of Vibration and Acoustics. 137**:** 041017-041017.

Pei, S., J. Berman, K. Ryan, J. Ricles, R. Sause, J.D. Dolan and J.W. van de Lindt (2018). Natural Hazards Engineering Research infrastructure (NHERI) Tall Wood Project. Golden, Colorado, Colorado School of Mines. 2018.

Pei, S., J. Berman, J.D. Dolan, J.W. van de Lindt, J. Ricles, R. Sause, H.-E. Blomgren, M. Popovski and D.R. Rammer (2014). Progress on the development of seismic resilient Tall CLT Buildings in the Pacific Northwest. Proceedings of the 2014 World Conference on Timber Engineering, Quebec City, Canada.

Pei, S., J.W. van de Lindt, M. Popovski, J.W. Berman, J.D. Dolan, J. Ricles, R. Sause, H.-E. Blomgren and D.R. Rammer (2016). Cross-Laminated Timber for Seismic Regions: Progress and Challenges for Research and Implementation. In: Journal of Structural Engineering. 142**:** E2514001.

Pei, S., J.W. van de Lindt, A. Barbosa, J. Berman, E. McDonnell, J.D. Dolan, R.B. Zimmerman, R. Sause, J. Ricles and K. Ryan (2018). Full-Scale Shake Table Test Of Mass-Timber Building With Resilient Post-Tensioned Rocking Walls. World Conference on Timber Engineering. Seoul, Republic of Korea.

TRADA (2009). Stadthaus, Murray Grove.

Zimmerman, R.B. and E. McDonnell (2017). Framework - A tall re-centering mass timber building in the United States. Joint 2017 New Zealand Society for Earthquake Engineering Annual Conference and the Anti-Seismic Systems International Society's 15th World Conference. Wellington, New Zealand.

Zimmerman, R.B. and E. McDonnell (2018). Framework - Innovation in Re-Centering Mass Timber Wall Buildings. 11th National Conference in Earthquake Engineering. Los Angeles, CA.

Marco Lo Ricco, P.E., S.E. - Ph.D. Candidate, Department of Civil and Environmental Engineering, University of Wisconsin-Milwaukee, P.O. Box 784, Milwaukee, WI 53201, mloricco@uwm.edu

Dr. Al Ghorbanpoor, P.E. - Professor, University of Wisconsin-Milwaukee, P.O. Box 784, Milwaukee, WI 53201, algh@uwm.edu

Dr. Shiling Pei, P.E. - Associate Professor, Department of Civil and Environmental Engineering, Colorado School of Mines, 1500 Illinois St., Golden, CO 80401, spei@mines.edu

Doug Rammer, P.E. - Research General Engineer, USDA/US Forest Service Forest Products Laboratory, One Gifford Pinchot Drive, Madison, WI 53726, drammer@fs.fed.us

Marshall Begel, P.E. - General Engineer, USDA/US Forest Service Forest Products Laboratory, One Gifford Pinchot Drive, Madison, WI 53726, mbegel@fs.fed.us

James Bridwell, M.S. - General Engineer, USDA/US Forest Service Forest Products Laboratory, One Gifford Pinchot Drive, Madison, WI 53726, jbridwell@fs.fed.us

Reid B. Zimmerman, P.E., S.E. - Associate, KPFF Portland, 111 SW Fifth Avenue, Suite 2500, Portland, OR 97204, Reid.Zimmerman@kpff.com

Improving the Accuracy of Wood Diaphragm Deflection Estimates

John W. Lawson, P.E., S.E.

Abstract:

Estimating horizontal deflections of diaphragms comprised of wood structural panels during wind and earthquakes is important for serviceability considerations, building separations and setbacks, and structural integrity evaluation in buildings with large span diaphragms. In smaller light-frame wood buildings, establishing the flexibility of diaphragms relative to adjacent shear walls or frames is necessary to properly classify whether a flexible, rigid or semi-rigid diaphragm approach is valid. Unfortunately, the wood diaphragm deflection equations in both the United States (US) SDPWS-2015 and Canadian CSA 086-14 wood-based structural design standards can often overestimate diaphragm deflections, leading to unnecessarily large building separations, property line setbacks or improper classification of flexible diaphragm behavior. Furthermore, researchers often use these equations to develop stiffness relationships within their numerical building models for dynamic analyses, and the inaccuracies posed by these equations will jeopardize the accuracy of their research results. Two primary culprits of this inaccuracy are associated with the simplification of the non-linear shear deformation and the original derivation estimating the panel perimeter-nail slip contribution. In this paper, the current wood panel diaphragm deflection equation is evaluated, and a new nail-slip contribution formula is mathematically derived that appropriately considers the nail slip contribution for a variety of situations including different panel orientations, different panel sizes, various nail spacings around the same panel, and variable non-linear nail-slip behavior within the same panel. Findings suggest that the current approach significantly underestimates stiffness.

Background

The computation of wood diaphragm deflections is becoming more commonplace as a heighten awareness of wind and seismic concerns exists now more than ever. Diaphragm deflections are routinely computed to establish building setbacks from property lines, building separations from each other, investigation of structural integrity, deformation compatibility, and/or $P\Delta$ building stability. Here an overestimation of diaphragm deflection leads to conservative results. However, an overestimation of diaphragm deflection will be problematic when establishing whether a diaphragm is appropriately modeled as flexible or rigid, or unconservative when establishing pseudo-lateral design forces from spectral response as done in ASCE's design standard *Seismic Rehabilitation of Existing Buildings* (ASCE 41-13) (ASCE 2013).

The current approach to computing diaphragm deflections was first developed by Countryman (1952) and contains a number of simplistic and conservative assumptions.

Computing Wood Diaphragm Deflections

Equation (1) is a 3-term equation from the American Wood Council's *Special Design Provisions for Wind and Seismic* (SDPWS) (AWC 2015) and has been the industry standard for estimating diaphragm deflections under uniformly distributed loading since the 2001 edition.

$$\delta_{dia} = \frac{5vL^3}{8EAW} + \frac{0.25vL}{1000G_a} + \frac{\sum(x\Delta_c)}{2W} \qquad \text{Equation (1)}$$

continued on next page

where:

v = induced maximum unit shear calculated at boundary, plf

L = diaphragm dimension perpendicular to the direction of the applied force, ft

E = modulus of elasticity of diaphragm chords, psi

A = area of diaphragm chord, in^2

W = width of diaphragm in direction of applied force, ft

G_a = apparent diaphragm shear stiffness, kips/in

x = distance from chord splice to nearest diaphragm support, ft

Δ_c = diaphragm chord splice slip at the induced unit shear, in

It is a simplification of the 4-term Equation (2) currently found in the SDPWS Commentary, and found in published standards since first introduced by Countryman (1952).

$$\delta_{dia} = \frac{5vL^3}{8EAW} + \frac{vL}{4G_v t_v} + 0.188Le_n + \frac{\sum(x\Delta_c)}{2W}$$

Equation (2)

where:

$G_v t_v$ = shear stiffness, lbs/inch of panel depth

e_n = nail slip, in

The first term of this equation estimates the flexural deformation of the wood diaphragm, the second term estimates the shear deformation of the wood structural panels, the third term estimates the deformation associated with nail slip, and the fourth term estimates the deformation effects from flexural chord connection slip. The second and third terms of Equation (2) are simplified into a combined second term in Equation (1). Because of the nonlinearity of the nail-slip term, only at the design level shear are the two equations calibrated to be equivalent; thus, Equation (1) can significantly overestimate diaphragm deflections compared with the more detailed approach in Equation (2).

Countryman developed Equation (2) using a mathematical derivation following general mechanics of materials. However, practitioners will significantly underestimate the diaphragm's stiffness when neglecting other potential chord elements, or assuming plywood usage instead of oriented strand board (OSB). Also, today's large buildings usually have multiple zones of different nailing patterns, and techniques have been established on computing these diaphragm deflections (Skaggs 2004; Lawson 2013).

Contribution due to Nail Slip

Because of its nonlinearity, the most difficult contribution to accurately estimate is the diaphragm's deflection due to the slip of nails around the panel edges. The nail-slip contribution (Equation 3) was derived only considering situations where the same nail spacing occurs around all edges of each 4-ft x 8-ft panel.

$$\Delta_n = 0.188Le_n \qquad \text{Equation (3)}$$

Today's blocked diaphragms typically have tighter nailing along continuous edges, a common design requirement under AWC SDPWS Tables 4.2A and 4.2B for all but the lightest nailed diaphragms. Additionally, diaphragms using 4-ft x 10-ft or larger panels are not uncommon. These situations cause Equation (3) to underestimate stiffness. It is desirable to derive a more widely applicable nail-slip contribution equation to minimize overestimating deflections and underestimating pseudo-lateral seismic forces.

Countryman's derivation approach does not lend itself to easily address varying nail spacings or panel sizes; however, a subsequent derivation approach presented in ATC 7's Appendix A (ATC 1981) does and will be used here to develop a new nail-slip contribution equation. It is important to note that the original derivations by Countryman and ATC 7 contain significant mathematical errors (Walford 1981; Tissell 1981), and were later corrected revising the previous $0.094Le_n$ to $0.188Le_n$. The derivation that follows is suitable to replace that in ATC 7.

continued on next page

First, recognize that the nail slip term can be divided into two separate contributions: a translating panel contribution and a rotating panel contribution (See Figures 1 and 2). The translational contribution Δ'_n results from nail slip on the panel edges parallel to the applied diaphragm load direction, and the rotational contribution Δ''_n results from nail slip on the panel edges perpendicular to the applied diaphragm load direction. The two contributions add directly together.

$$\Delta_n = \Delta'_n + \Delta''_n \qquad \text{Equation (4)}$$

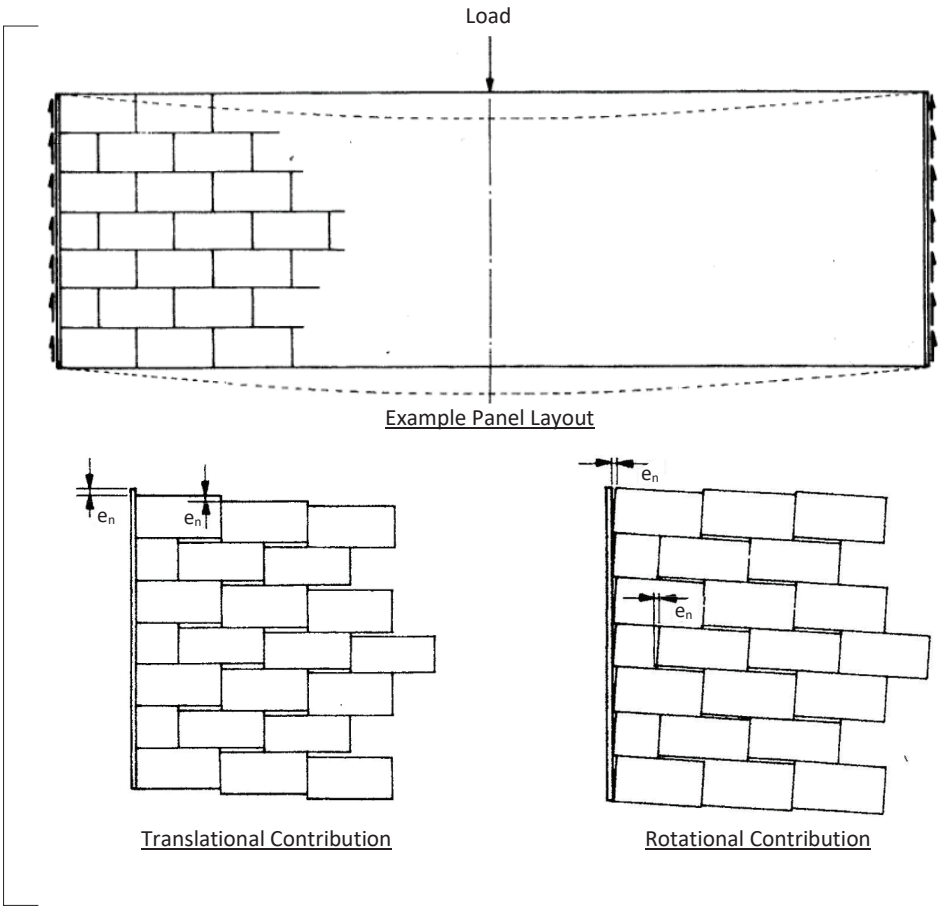

Figure 1: Nail-Slip Contributions to Diaphragm Deflection (Source: ATC 7)

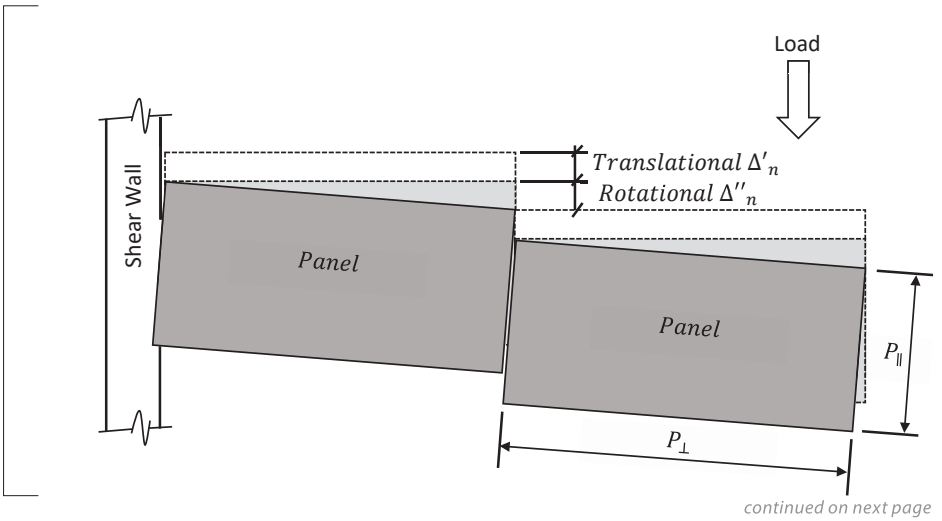

Figure 2: Panel translational and rotational components (exaggerated)

continued on next page

Consider the following definitions:

$P_{\parallel}$ = Panel dimension parallel to diaphragm load direction (same units as L)

$P_{\perp}$= Panel dimension perpendicular to diaphragm load direction (same units as L)

$S_{\parallel}$= Nail spacing on panel edges parallel to diaphragm load direction (inches)

$S_{\perp}$= Nail spacing on panel edges perpendicular to diaphragm load direction (inches)

$k=S_{\parallel}/S_{\perp}$ (ratio of edge nail spacings)

$V_{n\parallel}$= Shear per nail along panel edge parallel to diaphragm load direction (lbs per nail)

$V_{n\perp}$= Shear per nail along panel edge perpendicular to diaphragm load direction (lbs per nail)

L= Diaphragm span (measured perpendicular to diaphragm load direction) (same units as $P_{\parallel}$ and $P_{\perp}$)

x= Exponent on shear per nail V_n variable in SDPWS Table C4.2.2D

y= Denominator coefficient within nail slip term e_n in SDPWS Table C4.2.2D

$e_{n\parallel}$= nail slip based on $V_{n\parallel}$ shear per nail along panel edge parallel to diaphragm load direction

$e_{n\perp}$= nail slip based on $V_{n\perp}$ shear per nail along panel edge perpendicular to diaphragm load direction

Translational Contribution Δ'_n

Nails along opposite panel edges parallel to the diaphragm's loaded direction will slip in equal and opposite directions of $e_{n\parallel}$ and therefore the underlying frame will shift across the panel's length 2 $e_{n\parallel}$ (See Figure 2). This amount of translational movement occurs at every panel.

For a diaphragm with a concentrated load at midspan, the diaphragm experiences constant shear at each side of the applied load. For this situation, Δ'_n is the slip per panel multiplied by the number of panels to midspan

$$\Delta'_n = 2e_{n\parallel}\frac{L/2}{P_{\perp}} = \frac{e_{n\parallel}L}{P_{\perp}} \qquad \text{Equation (5)}$$

Rotational Contribution Δ''_n

Nails along opposite panel edges perpendicular to the diaphragm's loaded direction will slip in equal and opposite directions ($e_{n\perp}$) allowing a panel rotation. $e_{n\perp}$ is affected by the panel's aspect ratio $P_{\perp}/P_{\parallel}$ and nail spacing $S_{\perp}$. Figure 3 provides the panel edge shear relationship for equilibrium used in the derivation.

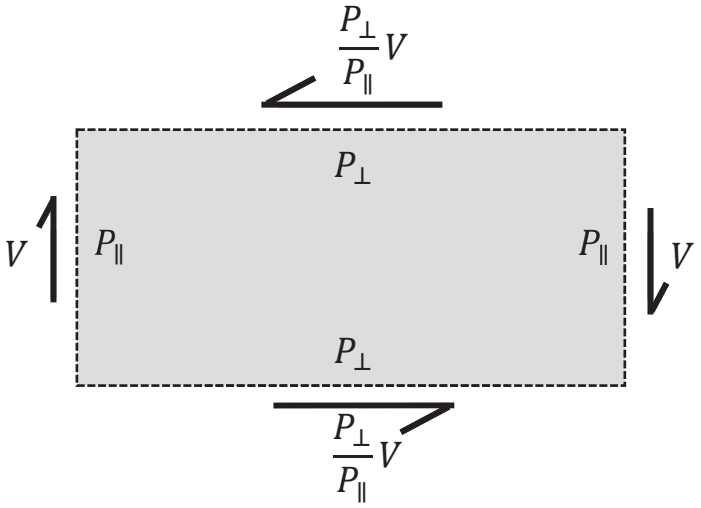

Figure 3: Panel edge shears for any rectangular shape

The general format for nail slip e_n from SDPWS Table C4.2.2D is:

$$e_n = \left(V_n/_y\right)^x$$

Thus

$$e_{n\perp} = \left(V_{n\perp}/_y\right)^x \qquad \text{Equation (6)}$$

The load per nail $V_{n\perp}$ is the shear along the perpendicular edge from Figure 3 divided by the number of nails:

$$V_{n\perp} = \frac{\frac{P_{\perp}}{P_{\parallel}}V}{P_{\perp}/_{S_{\perp}}} = V\frac{S_{\perp}}{P_{\parallel}}$$

Rearranging and substituting $kS_{\parallel}$ for $S_{\perp}$ the following is obtained:

$$V_{n\perp} = k\left(\frac{VS_{\parallel}}{P_{\parallel}}\right) \qquad \text{Equation (7)}$$

It is recognized that:

$$V_{n\parallel} = \frac{VS_{\parallel}}{P_{\parallel}} \qquad \text{Equation (8)}$$

continued on next page

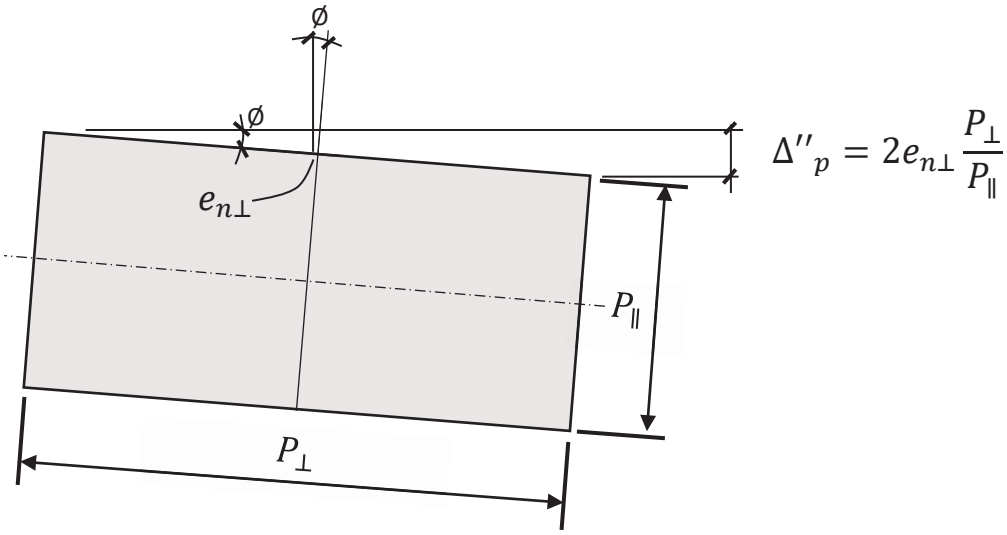

Figure 4: Rotational contribution per panel

Substituting Equation (8) into (7):

$$V_{n\perp} = kV_{n\parallel} \qquad \text{Equation (9)}$$

Substituting Equation (9) into (6)

$$e_{n\perp} = \left({}^{kV_{n\parallel}}/_{y}\right)^x = k^x\left({}^{V_{n\parallel}}/_{y}\right)^x = k^x e_{n\parallel}$$

Equation (10)

Using the theorem of similar triangles in Figure 4, the rotational contribution per panel Δ''_p is found.

$$\text{Rotational offset per panel } \Delta''_p = e_{n\perp}\frac{P_\perp}{P_\parallel/2} = 2e_{n\perp}\frac{P_\perp}{P_\parallel}$$

Equation (11)

Substituting Equation (10) into (11)

$$\text{Rotational offset per panel } \Delta''_p = 2k^x e_{n\parallel}\frac{P_\perp}{P_\parallel}$$

For a diaphragm with a concentrated load at midspan, the diaphragm experiences constant shear at each side of the applied load. For this situation, Δ''_n is the rotational offset per panel multiplied by the number of panel lengths to midspan.

The number of panel lengths to midspan $= \frac{L/2}{P_\perp}$

Therefore,

$$\Delta''_n = 2k^x e_{n\parallel}\frac{P_\perp}{P_\parallel}\frac{L/2}{P_\perp} = e_{n\parallel}L\frac{k^x}{P_\parallel} \qquad \text{Equation (12)}$$

Combining the two contributions of Equation (5) and Equation (12) into Equation (4):

$$\Delta_n = \Delta'_n + \Delta''_n = \frac{e_{n\parallel}L}{P_\perp} + \frac{e_{n\parallel}L}{P_\parallel}k^x = e_{n\parallel}L\left(\frac{1}{P_\perp} + \frac{k^x}{P_\parallel}\right)$$

Equation (13)

Equation (13) provides the third term nail-slip contribution when the diaphragm is loaded with constant shear from a midspan concentrated load. For a uniformly distributed loaded diaphragm, the shear varies linearly. Countryman's derivation for Equation (2) assumes the diaphragm's average nail slip is directly proportional to the average diaphragm shear. However, the nail slip actually varies nonlinearly with a linear shear variation, underestimating the stiffness somewhat, but this error is reduced in diaphragms with multiple nailing pattern zones that reduce nailing proportionally to the reduced shear. The SDPWS defines e_n as the nail slip at the boundary of a uniformly loaded diaphragm, thus e_n is divided by two to obtain the average.

$$\Delta_n = \frac{e_{n\parallel}L}{2}\left(\frac{1}{P_\perp} + \frac{k^x}{P_\parallel}\right) \quad \text{for uniformly loaded diaphragm}$$

Equation (14)

For a common 4-ft x 8-ft panel with uniform nailing on all panel edges, Equation (14) becomes:

$$\Delta_n = \frac{e_{n\parallel}L}{2}\left(\frac{1}{8} + \frac{1^x}{4}\right) = 0.188Le_{n\parallel} \qquad \text{Equation (15)}$$

continued on next page

The results from Equation (15) for nail slip contribution matches Equation (3), thus suggesting its validity. This equation is applicable regardless of the moisture content of the lumber during fabrication as long as the correct e_n and x terms are pulled from SDPWS Table C4.2.2D.

By ignoring situations with special continuous edge nail spacing and panel sizes larger than 4-ft x 8-ft, Equation (15) will always overestimate the diaphragm nail-slip contribution. Table 1 reports the discrepancy as a percentage of error between the current SDPWS nail-slip estimate within Equation (2) and the more refined approach in Equation (14). This same error is embedded in G_a of Equation (1). In some situations, the SDPWS nail-slip contribution estimate is 368% or 4.7 times greater than computed with Equation (14). Additionally, the panel layout case (Plate 1) can play a significant role. The layout cases shown are lettered by the author because they are different than the numbered layout cases within SDPWS Tables 4.2A and 4.2B.

Equation (16) is recommended for researchers and practitioners who are looking for a more refined approach to computing diaphragm deflections by considering the reduced nail slip effects from tighter continuous edge nailing and larger sized panels.

$$\delta_{dia} = \frac{5vL^3}{8EAW} + \frac{vL}{4G_v t_v} + 0.5\left(\frac{1}{P_\perp} + \frac{k^x}{P_\parallel}\right) Le_{n\parallel} + \frac{\sum(x\Delta_c)}{2W}$$

Equation (16)

Concluding remarks:

The available design equations to estimate diaphragm deflections have made simplifications at the expense of overestimating diaphragm deflections. Design engineers applying the SDPWS diaphragm deflection equations are likely to overestimate building separations and setbacks, while researchers or retrofit engineers are likely to underestimate building stiffness and pseudo-lateral forces. This paper provides recommendations to increase the accuracy of estimating diaphragm

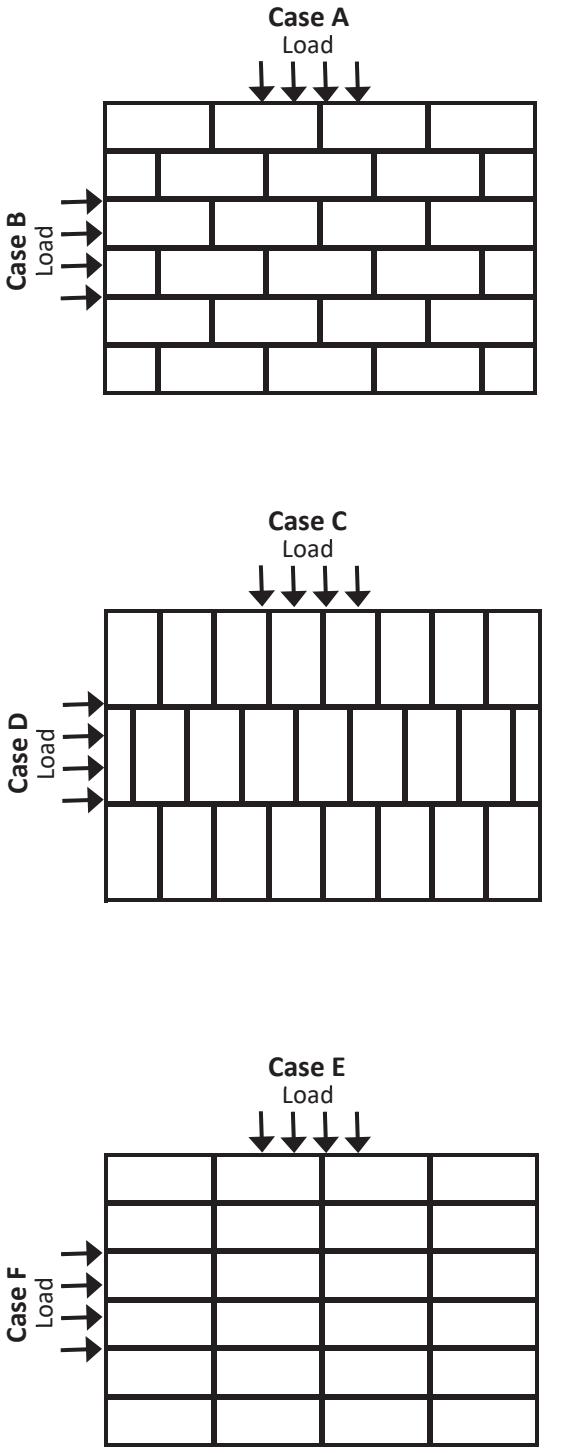

Plate 1: Panel layout cases for determination of nail slip contribution

continued on next page

Table 1 - Percentage of nail-slip error using the SDPWS's current 0.188 coefficient compared with Equation (14)

Panel Layout Configu-ration	Nail Size	SDPWS TABLE 4.2A (Blocked Diaphragm) Nail Spacings Continuous Edges / Other Edges				SDPWS TABLE 4.2B (High Load Diaphragm) Nail Spacings Continuous Edges / Other Edges			
		6″ / 6″	4″ / 6″	2.5″ / 4″	2″ / 3″	4″ / 6″	4″ / 4″	2.5″ / 4″	2.5″ / 3″
A & B	6d	0%	93%	107%	93%				
	8d	0%	89%	103%	89%				
	10d	0%	97%	111%	97%	97%	0%	111%	43%
C & D	6d	0%	32%	35%	32%				
	8d	0%	31%	34%	31%				
	10d	0%	33%	36%	33%	33%	0%	36%	18%
E & F	6d	0%	259%	339%	259%				
	8d	0%	241%	314%	241%				
	10d	0%	278%	368%	278%	278%	0%	368%	82%

Notes:

1. Coefficients tabulated assume diaphragm is comprised of 4x8 panel sizes and fabricated dry.
2. All continuous edges have nail spacing associated with "continuous edges parallel to the load" regardless of the load direction as is commonly specified in construction documents. This affects Cases A, C, E, F.
3. Error percentages will increase for panels larger than 4x8.

deflections and stiffness, and has derived a new equation for use that accounts for diaphragm deflections attributed to nail slip considering panel sizes, panel orientation, and the increased nailing at continuous edges.

References

ASCE, 2013. *Seismic Evaluation and Retrofit of Existing Buildings* (ASCE 41-13). American Society of Civil Engineers, Reston, VA.

ATC, 1981. *Guidelines for the Design of Horizontal Wood Diaphragms* (ATC-7), by Applied Technology Council, Berkeley, CA, September 1981

AWC 2015. *Special Design Provisions for Wind & Seismic with Commentary* (SDPWS), American Wood Council, Leesburg, VA.

Countryman, David; 1952. "Lateral Tests on Plywood-Sheathed Diaphragms," *Laboratory Report No. 55*, Douglas Fir Plywood Association.

Lawson, John; 2013. *Seismic Design of Timber Panelized Roof Structures,* Woodworks, Washington, DC.

Skaggs, Thomas; and Martin, Zeno; 2004. "Estimating Wood Structural Panel Diaphragm and Shear Wall Deflection," *Practice Periodical on Structural Design and Construction,* Volume 9, Issue 3, pp. 136-141, American Society of Civil Engineers, Reston, VA.

Tissell, John; 1981. Interoffice memo, June 8, 1981.

Walford, G.B.; 1981. Letter from G.B. Walford to J.R. Tissell, American Plywood Association, Tacoma, WA, April 30, 1981.

John W. Lawson, P.E., S.E. is Associate Professor, Architectural Engineering at California Polytechnic State University in San Luis Obispo, California. jwlawson@calpoly.edu